Critical period signalling directs nervous system development through mitochondrial ROS and HIF-1α.

Daniel Sobrido-Cameán[1]*, Bramwell Coulson[2], Matthew C.W. Oswald[1], Tom Pettini[1], Richard A. Baines[2]*, Matthias Landgraf[1]*.

[1]Department of Zoology, University of Cambridge, CB2 3EJ, Cambridge, UK

[2] Division of Neuroscience, School of Biological Sciences, Faculty of Biology, Medicine and Health, University of Manchester, Manchester Academic Health Science Centre, Manchester, M13 9PT, UK

*** Correspondence:**
Corresponding Authors
ds918@cam.ac.uk, ml10006@cam.cam.uk, Richard.Baines@manchester.ac.uk

Keywords: critical period, nervous system, development, *Drosophila melanogaster*, mitochondria, reactive oxygen species, reverse electron transport, HIF-1alpha, temperature.

Abstract

Critical periods of nervous systems development are phases of heightened plasticity, which facilitate experience-dependent network tuning, but also make them vulnerable to perturbations, which can result in lasting mal-adjustment. In the case of cold-blooded animals (poikilotherms), variations in temperature impact on nervous system development, causing both structural and functional changes that persist and alter behaviour. Here, we have identified the underlying signalling framework. Harnessing the well-defined critical period of the fruit fly embryo as an experimental, genetically tractable model, we asked how heat stress leads to lasting changes in synapse size and composition, neuronal excitability and animal behaviour. We established that heat stress leads to the generation of reactive oxygen species (ROS) within mitochondria, by reverse electron transport. This mitochondrial ROS signal is then transmitted to the nucleus by the *Drosophila* homologue of the highly conserved hypoxia inducible factor-1alpha (HIF-1α). The mitochondrial ROS-HIF-1α signalling pathway that we have identified is required for cells to respond to developmental heat stress. It is also sufficient to cell autonomously specify those changes in neuronal properties and animal behaviour, when activated during, but not outside the embryonic critical period.

Introduction

Most animals, including insects, amphibians and reptiles, are not warm blooded and have limited ability to regulate their internal temperature. Their development, particularly of their nervous systems, is therefore vulnerable to changes in environmental temperature, which affects all biological processes. In the developing brains of bees, ants and fruit flies, changes in rearing temperature leads to structural changes in cell number and connectivity[1–5], with changes in sensory processing, learning and behaviour[1,4–9]. To regulate brood temperature, many social insect have evolved complex behaviours ranging from nest design to active cooling and heating, or rhythmic daily movement of pupae to warmer and cooler locations[10]. In amphibians and reptiles, variations in developmental temperature also cause changes in behaviour[11,12]. Specific phases of nervous system development are particularly sensitive to temperature and activity perturbations, referred to as 'sensitive' or 'critical' periods of development[1,13–16]. For example, we identified a 2-hour critical period window in late embryogenesis of the *Drosophila melanogaster* (fruit fly) embryo, during which changes in developmental temperature or neuronal activity lead to the emergence of sub-optimal neuronal properties, reducing locomotor speed and making animals more susceptible to seizures[15,17,18].

Though many aspects nervous systems, which are impacted by transient temperature experiences during a critical period of development, have been studied, the signalling pathways and molecular mechanisms are not known. In this study, we set out to identify those mechanisms. To do so, we took advantage of the well-defined critical period of the *Drosophila* embryo[15]. Specifically, this model system allows genetic manipulations to be targeted to single neurons or muscles, to identify cell-autonomous signals that cell-selectively rescue or mimic the effects of a systemic temperature experience. Temporal control over gene expression allowed us to identify pathways required specifically during the critical period, but which had no lasting effect on developmental outcomes when applied after this window of elevated plasticity.

The locomotor network of the *Drosophila* larva forms during embryonic stages and is particularly sensitive to activity perturbations in late embryonic stages, when the network becomes synaptically active[13–15,19–21]. Activity manipulations during a defined 2-hour critical period, irrespective of whether those increase or decrease network activity, lead to lasting changes in network performance that manifest in reduced crawling speed and network instability[15,17,21]. Nitric oxide signalling has been identified as downstream of neuronal activity, and Baines and co-workers proposed that during the critical period, the overall balance of excitatory and inhibitory activity is integrated by the developing network to shape its properties, and thus its performance[18]. A key outcome of critical period adjustments has been suggested to be the specification of network setpoints[15,22]. If correct, this could explain why persisting plasticity mechanisms are often unable to fully correct errors induced by a critical period perturbation. We found that changes in ambient temperature correlate with changes in locomotor network activity, and that heat stress

experience during the embryonic critical period largely phenocopies network activity manipulations during this developmental phase[15,17,18,23].

In addition to affecting neuronal activity, temperature affects biochemical reactions in general, and metabolic and mitochondrial processes in particular[24]. In *Drosophila,* a heat stress of 32˚C, which is ecologically relevant[16], causes a reversal of the flow of electrons within the mitochondrial electron transport chain (ETC), from Complex-II back to Complex-I. This so-called reverse electron transport (RET) leads to the production of reactive oxygen species (ROS) at Complex-I, due to the partial reduction of oxygen and the formation of superoxide anions. In *Drosophila*, as well as mouse, RET-generated ROS have been linked to increased lifespan and improved stress resistance[25–29]. Here, we identified RET-based generation of ROS at mitochondrial Complex-I as the fundamental signalling pathway by which heat stress during the critical period changes the subsequent development of muscles and neurons.

Seeking to understand how such mitochondrial ROS could direct gene expression, we identified the conserved Hypoxia-inducible factor 1 alpha (HIF-1α)[30–32]. The molecular mechanisms governing the hypoxia-responsive system are highly conserved, mediated by multiple HIFs in mammals, but simplified in *Drosophila* with only a single HIF homologue, called *similar (sima)*. HIF-1α is a sensor for oxygen levels, sensitive to ROS levels, and is a regulator of glycolytic enzyme expression[33]. During normal development, HIF-1α regulates many processes, including neurogenesis, angiogenesis, and cell survival[34–36]. Its dysregulation is linked to a range of cancers[37]. Here, we identified HIF-1α acting downstream of mitochondrial RET-generated ROS, as a transducer of this signal to the nucleus. In summary, we discovered a cell-autonomous signalling pathway that senses heat stress during the critical period, specifying the development of cellular properties and thus synaptic terminal size and composition, network output and stability, and behaviour.

Results

Mitochondrial ROS are plasticity signals during the embryonic critical period

We recently found that a transient heat stress of 32°C, when experienced during the embryonic critical period (17 -19 hr after egg laying), leads to reduced network stability, making larvae more susceptible to seizures, altered neuronal excitability and crawling behaviour[17]. To identify the underlying signalling pathways that turn critical period perturbations into lasting changes in nervous system development and function, we used the *Drosophila* larval NMJ as a proven experimental model[38–40]. Structural changes are evident at the NMJ in the form of presynaptic terminal overgrowth (Figure 1A-C). The postsynaptic muscle responds with a decrease in the postsynaptic high-conductance glutamate receptor subunit, GluRIIA (Figure 1D), but not the lower conductance subunit, GluRIIB (Figure 1E).

The NMJ overgrowth phenotype resembled outcomes from neuronal overactivation-induced reactive oxygen species (ROS) signalling, which we had previously studied[41,42]. We therefore asked if mitochondrial ROS might be involved. To test this, we genetically manipulated mitochondrial ROS levels in embryonic stages only, selectively within a single muscle per half segment; the most dorsal muscle, dorsal acute 1 (DA1). Mis-expression of the mitochondrially targeted ROS scavenger, mito-Catalase or Perexiredoxin-3 (Prx3), in muscle DA1, cell-selectively rescues the NMJ overgrowth (Figure 1C) and GluRIIA phenotypes that otherwise result from a systemically experienced heat stress during the embryonic critical period (Figure 1D). While at the control temperature of 25°C, no lasting effects result from these transient genetic manipulations (Figure 1).

Mitochondria can generate ROS through various means, notably at Complex-I and Complex-III of the electron transport chain. 32°C heat stress causes ROS generation at Complex-I in adult *Drosophila*, via reverse flow of electrons from Complex-II back to Complex-I, called 'reverse electron transport', or 'RET'[27]. To test if 32°C heat stress in embryos causes RET-generated ROS in mitochondria, we cell-selectively knocked down a subunit of Complex-I, ND-75, instrumental for RET-generated ROS. Complementing, we neutralised RET-generated ROS by mis-expression of alternative oxidase (AOX), an enzyme found in the inner mitochondrial membrane of many organisms, though not vertebrates or insects[43–46]. In mitochondria, AOX acts as a bypass that transfers electrons from ubiquinone to oxygen, independent of Complexes-I and -III, thereby reducing the probability of electron backflow through these complexes and subsequent ROS production by RET[27,47–49]. When we targeted either of these genetic manipulations to muscle DA1 during embryonic stages, they rescued the critical period heat stress phenotype (Figure 1). Under control conditions of 25°C both manipulations were neutral, leaving NMJ development unaffected (Figure 1). Together, these results show that during the embryonic critical period, RET-generated ROS at Complex-I are necessary for heat stress to effect a lasting change in subsequent NMJ development.

We next asked if ROS generated by Complex-I might be sufficient for inducing lasting changes, in absence of systemic heat stress, which might affect many other aspects of biology. To test this, we cell-selectively induced RET-ROS at Complex-I by mis-expression of NADH dehydrogenase 1 (Ndi1) from yeast. Ndi1 transfers electrons from NADH to the CoQ pool. This can lead to the accumulation of reduced CoQ and transfer of electrons to Complex-I, causing RET and associated ROS generation at Complex-I[28]. Mis-expression of Ndi1 in *Drosophila* had previously been shown to increase ROS production in a way indistinguishable from RET[28]. Indeed, we found that transient embryonic mis-expression of Ndi1 in muscle DA1, at the control temperature of 25°C, cell-selectively phenocopies the characteristic critical period heat stress phenotype of NMJ overgrowth (Figure 2A-C) and reduced GluRIIA levels (Figure 2E). Thus, our results show that in postsynaptic muscles during the embryonic critical period RET-generated ROS are mitochondrial signals that are both necessary and sufficient for inducing lasting change to NMJ development.

Mitochondrial RET-generated ROS are critical period signals for NMJ development.

Because synapse development depends on the close interactions between pre- and postsynaptic partners, we next tested the roles of these mitochondrial signals in the presynaptic motoneuron, called 'aCC', whose NMJ forms on muscle DA1. We identified a transgenic line that transiently targets Gal4 expression to the aCC presynaptic motoneuron selectively during embryonic stages, including the critical period. Using this aCC-Gal4 [1] genetic tool (aka *RN2-O-Gal4*), we found that mis-expression of AOX in the aCC motoneurons, to neutralise RET-induced ROS generation at Complex-I, was sufficient to rescue the NMJ overgrowth that normally results from embryonic experience of 32°C heat stress (Figure 3 A-C). Increases in NMJ size led to proportionate increases in the number of presynaptic active zones, the sites of vesicular neurotransmitter release (Figure 3D). Active zone number was also fully rescued by simultaneous embryonic mis-expression of AOX in the aCC motoneurons (Figure 3D). Conversely, transient embryonic generation of RET-ROS in the aCC motoneurons by mis-expression of Ndi1 was sufficient to cell-selectively mimic the critical period heat stress phenotype (Figure 3B-D).

To test the importance of developmental timing during which transient RET-generated ROS can cause such lasting change, we contrasted the effects of transient genetic manipulations of aCC motoneurons, during the late embryonic stage, including the critical period, *versus* after closing of the critical period, during the first larval stage. We achieved temporal and spatial control of Gal4 expression by combining two transgenes: another, independently generated expression line, aCC-Gal4 [2] (aka *GMR96G06-Gal4*), which specifically targets Gal4 to the aCC motoneuron during embryonic and also larval stages[50,51], combined with a conditional Gal4 inhibitor from the recently published "AGES" system[52]. To induce Gal4 activity during the critical period, we fed auxin to gravid females, while for later expression, post critical period closing, we fed auxin to freshly hatched larvae for 24 hours. The results confirm that the timing of mitochondrial RET-generated ROS is important: only when cells generate these mitochondrial ROS signals during the embryonic phase, including the critical period, do those ROS cause lasting changes, in keeping with this being a sensitive or critical period of NMJ development (supplementary figure 1).

The conserved HIF-1α pathway transduces the mitochondrial ROS signal to the nucleus.

We next considered how mitochondrial ROS, which are triggered by heat stress, might effect changes to developmental outcomes. HIF-1α is a transcription factor that plays a central role in cellular response to hypoxia and other stresses, including oxidative stress[53]. First, we knocked down the single *Drosophila* homology of *HIF-1α*, *sima,* selectively in DA1 muscles while exposing embryos to 32°C during the critical period. This showed that HIF-1α is necessary during this window to cause heat stress-induced changes in NMJ development, namely overgrowth (Figure 4A-C) and a postsynaptic decrease of the GluRIIA receptor subunit (Figure 4D). Conversely, transient embryonic mis-expression of *HIF-1α* in

DA1 muscles, at the control temperature of 25°C, is sufficient to mimic those NMJ phenotypes (Figure 4). Under normoxic conditions, HIF-1α is continuously degraded by the proteasome, regulated via hydroxylation by the conserved prolyl hydroxylase, PHD (a single *Drosophila* homologue, *Hph/fatiga*). Hydroxylated HIF-1α is recognised by the E3 ligase complex substrate recognition subunit, von Hippel-Lindau (VHL), leading to HIF-1α ubiquitination and subsequent proteasomal degradation[54]. Mitochondrial ROS, including RET-generated, can inhibit PHD and thereby stabilize HIF-1α, also under normoxic conditions[31,55-58]. To further consolidate the role of HIF-1α signalling, we elicited transient stabilisation of HIF-1α in embryonic muscle DA1 at the control temperature of 25°C, via RNAi knockdown of HIF-1α degradation machinery components: the prolyl hydroxylase, PHD, or the VHL ubiquitin ligase complex substrate recognition subunit. Both these manipulations phenocopy the characteristic NMJ overgrowth phenotype (Figure 4).

To test the working model of HIF-1α signalling as downstream of mitochondrial RET-generated ROS, we used a genetic epistasis experiment: of inducing RET via mis-expression of Ndi1, while simultaneously knocking down the putative downstream acceptor, HIF-1α. We found that RET induction was no longer able to induce a change in larval NMJ development when HIF-1α was knocked down in the same cell (Figure 4). This confirms the working model of information flow from mitochondrial RET-generated ROS to nuclear HIF-1α.

Neuronal excitability and crawling speed are specified during the critical period by the mitochondrial ROS to HIF-1α signalling axis.

We next asked whether these structural changes that result from critical period plasticity have correlates in neuronal function and animal behaviour[17]. To this end, we generated whole cell patch clamp recordings from aCC motoneurons at the late larval stage. These showed that embryonic heat stress of 32°C caused a lasting reduction in excitability, while leaving cell size (assessed by membrane capacitance) and resting membrane potential unaffected (Figure 5A-D). We find that this effect of critical period heat stress experience, on reducing neuronal excitability, requires the RET-ROS - HIF-1α signalling axis. It is blocked when neutralising RET-ROS by simultaneous mis-expression of AOX. Conversely, induction of HIF-1α during the critical period is sufficient to induce this reduction in neuronal excitability at the control temperature of 25°C (Figure 5A-D). At the network level, we find that mitochondrial RET-ROS and HIF-1α signalling are also required and sufficient for critical period-regulated changes in locomotor network output. Transient induction of these signals in all embryonic neurons, at the control temperature, phenocopies the reduction in crawling speed that is also caused by critical period heat stress (Figure 5E). This effect of RET-ROS and HIF-1α signalling is specific to the critical period window, as manipulations outside this plastic period do not lead to lasting changes (supplementary figure 2).

We conclude that during the embryonic critical period, mitochondrial RET-generated ROS are instructive signals that are transmitted to the nucleus via the conserved transcriptional

regulator, HIF-1α. Only when activated during the embryonic critical period, does this signalling pathway alter the subsequent development of the nervous system, leading to changes in synaptic terminal growth, receptor composition, neuronal excitable properties and network output, as manifest by changes in larval crawling behaviour (Figure 6).

Discussion

Working with a simplified experimental system, we have identified a conserved signalling pathway from mitochondrial RET-generated ROS to HIF-1α, as instructive during a critical period of nervous system and muscle development in *Drosophila*. This provides a first mechanistic explanation for how heat stress experienced during this plastic phase effects a change in subsequent development, leading to altered neuronal properties and animal behaviour. By virtue of targeting genetic manipulations, transiently, to single cells *in vivo*, we were able to demonstrate that critical period responses are fundamentally cell intrinsic.

Environmental cues are integrated during critical periods and direct nervous system development

It has long been known that early life experiences are formative, due to their potential to impart lasting influence on nervous system function. Though critical periods have been most intensively studied in the context of activity-regulated sensory processing and cortical networks, it is possible that critical periods represent a fundamental process of nervous system development. For example, similar developmental windows of heightened vulnerability to disturbances have also been identified in mammalian locomotor systems[59], as well as in locomotor, visual and olfactory systems of zebrafish[60–64] and several insect species (ants, bees and *Drosophila*[1,1–5]). In fast developing organisms, opening of a critical period correlates with the phase when network activity transitions from unpatterned to patterned activity, and in the case of the locomotor network of the *Drosophila* embryo lasts only two hours[13–15,20,21,65]. In mammalian systems, critical periods are much more drawn out, lasting weeks in mouse and up to several years in humans[66]. Notwithstanding such differences, the neuronal activity-regulated processes of critical periods are remarkably similar across species; from GABAergic signalling during critical periods of visual system development[64], to the importance of the overall excitation:inhibition balance, also in the developing *Drosophila* locomotor network[18,20].

Here, we took advantage of a well-defined 2-hour critical period of the *Drosophila* locomotor network[15,18] to investigate how temperature is integrated as an important environmental cue. Having previously identified 32°C heat stress as an ecologically relevant stimulus that leads to lasting change in subsequent motoneuron development[17], we now identify the basic instructive signal elicited by this heat stress, namely mitochondrial ROS generated at Complex-I via reverse flow of electrons within the electron transport chain. The reasons why heat stress causes the reverse flow of electrons, whether it acts as a biophysical switch or as a result of temperature-induced changes in mitochondrial metabolism, needs to be

determined. In mammals, mitochondrial RET-generated ROS has been associated with ageing and expression of protective responses[27,67]. Whether this same signal is also responsible for the responses to developmental heat stress reported in ants[9], bees[3,7,8] or other parts and stages of the developing *Drosophila* nervous system[1,16], remains to be tested. Though we employed a stress signal in this study, to elicit a robust critical period response, temperature operates as a general environmental cue during nervous system development, at least in pokilothermic animals. Contrasting with this study, a cooler, non-stress temperature experience, during the pupal critical period of *Drosophila* nervous system development, leads to clear cellular effects; of reduced filopodial dynamics and consequent increase in synapse formation with concomitant changes in network connectivity and behaviour[1,5].

Critical period effects at the level of single cells

One of the strengths of the experimental system we used here, is that it allows studying critical period biology with single cell resolution *in vivo*. This simplifies establishing clear cause-effect relationships, which is more difficult with commonly used network-wide manipulations. Through cell-selective genetic manipulations of a single motoneuron or its target muscle we could phenotypically rescue individual cells from systemic heat stress manipulations. Thus, we demonstrated the cell-autonomous necessity of RET-generated mitochondrial ROS and HIF-1α signalling for heat stress-induced critical period plasticity. Conversely, we also showed cell-selective sufficiency of RET-ROS and HIF-1α signalling to phenocopy changes in NMJ development, though only when induced during the transient embryonic critical period, but not afterwards. We thus demonstrated conclusively *in vivo* that individual cells undergo their own, potentially cell type-specific, critical periods.

From a developmental perspective, this implies that different cell types might be integrated into circuitry in a sequential manner, for example based on birth order or maturation speed, thus facilitating more reproducible and robust network assembly. Across a developing nervous system, different regions are known to undergo their respective critical periods in sequence[66], which is mirrored at the cellular level within a given network. A recent study centred on developing mouse neocortex demonstrated the sequential maturation of two principal classes of inhibitory interneurons, and how this process directs network maturation[68].

Conserved mitochondrial-nuclear signalling directs critical period plasticity

Cells integrate internal (e.g. network activity) and external environmental cues (e.g. temperature) during a critical period. The identification of an instructive signal that is intimately linked to mitochondrial metabolism significantly adds to and complements a large body of work that has focused on activity-regulated processes[69,70]. How neuronal activity-regulated signalling and mitochondrial metabolism interlink, especially during critical periods of development, will be important to understand. We had previously shown that mitochondrial and NADPH oxidase-generated ROS are required for activity-regulated

neuronal plasticity outside the critical period[41,42,71]. Here, we identified a specific source of mitochondrial ROS, namely those generated at Complex-I via RET, which occurs when the coenzyme Q pool is reduced while the proton motif force is elevated[72]. A mitochondrial enzyme that is linked to the redox state of the coenzyme Q pool, dihydroorotate dehydrogenase (DHODH) has been identified as an important regulator of neuronal action potential firing rate, i.e. a determinant of the neuronal homeostatic setpoint[22,73]. Together with our findings here we speculate that mitochondrial metabolism might be central to critical period plasticity, potentially specifying neuronal homeostatic setpoints.

How might a transient perturbation during a critical period lead to lasting change? HIF-1α, a transcriptional regulator involved in the cellular response to stress, is typically degraded under normal oxygen concentrations. The model we propose is that mitochondrial ROS, including those generated by RET, transiently inhibit the degradation of HIF-1α, thus allowing HIF-1α to accumulate and translocate into the nucleus[31,31,55–58]. HIF-1α signalling is a known regulator of changes in cellular metabolism, for example promoting aerobic glycolysis in a range of cancers[74–76], as well as during normal development, when rapid tissue growth is required[34,77,78]. HIF-1α achieves this through a combination of direct regulation of gene expression, notably of metabolic enzymes, and epigenetic modifications, partly executed through histone acetyl transferases that act as co-factors[79–82]. In some forms of cancer, this is thought to create positive feedback loops, from elevated mitochondrial metabolism, to increased ROS production maintaining disinhibition of HIF-1α, which reinforces metabolic drive. It is therefore possible that transient HIF-1α signalling could initiate such metabolic-epigenetic feedback loops that could maintain a change in metabolic state, and thus also of neuronal growth and functional properties.

Materials and Methods

Drosophila rearing and stocks.

Drosophila stocks were kept on standard corn meal medium, at 25°C. For all experiments where crosses were necessary, stocks were selected and combined as a 1:2 ratio of Gal4-line males to UAS-line virgin females. See table 1 for the strains used.

Critical Period manipulations

Temperature manipulations: Embryos were harvested from 0 to 6 hours after egg lay at 25°C. Embryos were then shifted to their respective temperatures in incubators (25°C or 32°C) from for the remainder of embryogenesis. After all animals hatched, all were move back to 25°C until assayed in late larval stages (Figure 7).

Auxin feeding: Auxin (GK2088 1-Naphthaleneacetic acid potassium salt; Glentham) solution was mixed with melted molasses fly medium to achieve 5mM auxin concentration, poured into petri dish plates. For embryonic exposure to auxin, adult flies in mixed-sex laying pots

were fed on this food for 48 hours prior to egg collection. For larval exposure, freshly hatched larvae were fed on this food for 24 hours.

Dissections and immunocytochemistry

Flies were allowed to lay eggs on apple-juice agar based medium overnight at 25˚C. Larvae were then reared at 25°C on yeast paste, while avoiding over-crowding. Precise staging of the late wandering third instar stage was achieved by: a) checking that a proportion of animals from the same time-restricted egg lay had initiated pupariation; b) larvae had reached a certain size and c) showed gut-clearance of food (yeast paste supplemented with Bromophenol Blue Sodium Salt (Sigma-Aldrich)). Larvae (of either sex) were dissected in Sorensen's saline, fixed for 10 min at room temperature in Bouins fixative (Sigma-Aldrich), as previously detailed[42]. Wash solution was Sorensen's saline containing 0.3% Triton X-100 (Sigma-Aldrich) and 0.25% BSA (Sigma-Aldrich). Primary antibodies, incubated overnight at 10°C, were: Goat-anti-HRP Alexa Fluor 488 (1:1000; Jackson ImmunoResearch Cat. No. 123-545-021), Rabbit-anti-GluRIIB (1:1000; gift from Mihaela Serpe[83]), Mouse anti-GluRIIA (1:100; Developmental Studies Hybridoma Bank, Cat. No. 8B4D2 (MH2B)); Mouse anti-BRP (1:100; Developmental Studies Hybridoma Bank, Cat. No. nc82); secondary antibodies, 2 hr at room temperature: Donkey anti-Mouse StarRed (1:1000; Abberior, cat.no. STRED-1001); and goat anti-Rabbit Atto594 (1:1000; Sigma-Aldrich Cat No 77671-1ML-F). Specimens were cleared in 80% glycerol, overnight at 4°C, then mounted in Mowiol.

Image acquisition and analysis

Specimens were imaged using an Olympus FV3000 point-scanning confocal, and a 60x/1.3 N.A silicone oil immersion objective lens and FV31S-SW software. Confocal images were processed using ImageJ (to quantify GluRIIA and -B intensity) and Affinity Photo (Serif Ltd) to prepare figures. Bouton number of the aCC NMJ on muscle DA1 from segments A3-A5 was determined by counting every distinct spherical varicosity.

To quantify GluRIIA and -B fluorescence intensity a threshold image for each channel was used to generate an outline selection, which included only the postsynaptic glutamate receptor clusters. This outline was then applied to the original image to define the regions of interest for analysis. Fluorescence intensities for GluRIIA and GluRIIB channels was measured within these outlines. Data were exported into Excel and the intensity values normalised to the negative control condition (25°C through all embryogenesis).

Electrophysiology

Third instar (L3) larvae (of either sex) were dissected in a dish containing standard saline (135mM NaCl (Fisher Scientific), 5mM KCl (Fisher Scientific), 4mM $MgCl_2 \cdot 6H_2O$ (Sigma-Aldrich), 2mM $CaCl_2 \cdot 2H_2O$ (Fisher Scientific), 5mM TES (Sigma-Aldrich), 36mM sucrose (Fisher Scientific), pH 7.15) to remove the ventral nerve cord and brain lobes (CNS). The isolated CNS was then transferred to a droplet of external saline containing 200 μM Mecamylamine to block postsynaptic nACh receptors in order to synaptically isolate motor

neurons. CNSs were laid flat (dorsal side up) and glued (GLUture Topical Tissue Adhesive; World Precision Instruments USA) to a Sylgard-coated cover slip (1 to 2mm depth of cured SYLGARD Elastomer (Dow-Corning USA) on a 22 x 22mm square coverslip). Preparations were placed on a glass slide under a microscope (Olympus BX51-WI), viewed using a 60x water-dipping lens. To access nerve cell somata, 1% protease (Streptomyces griseus, Type XIV, Sigma-Aldrich, in external saline) contained within a wide-bore glass pipette (GC100TF-10; Harvard Apparatus UK, approx. 10 μm opening) was applied to abdominal segments, roughly between A5-A2 (Baines and Bate, 1998) to remove overlaying glia. Motoneurons were identified by anatomical position and relative cell size, with aCC being positioned close to the midline and containing both an ipsilateral and contralateral projection. Whole cell patch clamp recordings were made using borosilicate glass pipettes (GC100F-10, Harvard Apparatus) that were fire polished to resistances of 10 - 15MΩ when filled with intracellular saline (140 mM potassium-D-gluconate (Sigma-Aldrich), 2 mM $MgCl_2 \cdot 6H_2O$ (Sigma-Aldrich), 2 mM EGTA (Sigma-Aldrich), 5 mM KCl (Fisher Scientific), and 20 mM HEPES (Sigma-Aldrich), (pH 7.4). Input resistance was measured in the 'whole cell' configuration, and only cells that had an input resistance ≥ 0.5 GΩ were used for experiments. Cell capacitance and break-in resting membrane potential were measured for each cell recorded; only cells with a membrane potential upon break in of < -40 mV were analysed. Data for current step recordings were captured using a Multiclamp 700B amplifier (Molecular Devices) controlled by pCLAMP (version 10.7.0.3), via an analogue-to-digital converter (Digidata 1440A, Molecular Devices). Recordings were sampled at 20 kHz and filtered online at 10 kHz. Once patched, neurons were brought to a membrane potential of -60 mV using current injection. Each recording consisted of 20 x 4 pA (500 ms) current steps, including an initial negative step, giving a range of -4 to +72 pA. Number of action potentials were counted and plotted against injected current. Cell capacitance and membrane potential were measured between conditions to ensure that any observed differences in excitability were not due to differences in either cell size or resting state.

Larval crawling analysis

At the mid-third instar stage, 72 hours after larval hatching (ALH), larvae were rinsed in water and placed inside a 24cm x 24cm crawling arena with a base of 5mm thick 0.8% agarose gel (Bacto Agar), situated inside an incubator. Temperature was maintained at 25±0.5°C, reported via a temperature probe in the agar medium. Humidity was kept constant. Larval crawling was recorded using a frustrated total internal reflection-based imaging method (FIM) in conjunction with the tracking software FIMTrack (Risse et al., 2017, 2013) using a Basler acA2040-180km CMOS camera with a 16mm KOWA-IJM3sHC.SW-VIS-NIR Lens controlled by Pylon (by Basler) and Streampix (v.6) software (by NorPix). Larvae were recorded for 20 minutes at five frames per second.

Recordings were split into four 5-minute sections with the first section not tracked and analysed as larvae are acclimatising to the crawling arena. The remaining three sections were used to analyse crawling speed, with each larva sampled at most once per section. Crawling speed was calculated using FIMTrack software choosing crawling tracks that

showed periods of uninterrupted forward crawling devoid of pauses, turning or collision events. The distance travelled was determined via the FIMTrack output.

Statistical analysis

Statistical analyses were carried out using GraphPad Prism Software (Version 10.1.2). Datasets were tested for normal distribution with the Shapiro-Wilk Test. Normally distributed data were then tested with students t-test (for pairwise comparison). Normally distributed analysis for more than two groups was done with a one-way ANOVA and post hoc tested with a Tukey multiple comparison test. Non-normally distributed data sets of two groups were tested with Mann-Whitney U Test (pairwise comparison) and datasets with more than two groups were tested with a Kruskal Wallis ANOVA and post hoc tested with a Dunns multiple post hoc comparison test. For whole cell electrophysiology in aCC neurons, linear regression analysis was used to compare the intercepts between conditions, using a Bonferoni correction for multiple comparisons, resulting in an adjusted significance threshold of $p < 0.0083$. This analysis was restricted to the linear portions of the input-output curves. For all datasets mean and standard error of mean (SEM) are shown. Significance levels were * $p<0.05$; ** $p<0.01$; *** $p<0.001$; **** $p<0.0001$.

References

1. Kiral, F.R., Dutta, S.B., Linneweber, G.A., Hilgert, S., Poppa, C., Duch, C., Von Kleist, M., Hassan, B.A., and Hiesinger, P.R. (2021). Brain connectivity inversely scales with developmental temperature in Drosophila. Cell Rep. *37*, 110145. https://doi.org/10.1016/j.celrep.2021.110145.

2. Falibene, A., Roces, F., Rössler, W., and Groh, C. (2016). Daily Thermal Fluctuations Experienced by Pupae via Rhythmic Nursing Behavior Increase Numbers of Mushroom Body Microglomeruli in the Adult Ant Brain. Front. Behav. Neurosci. *10*. https://doi.org/10.3389/fnbeh.2016.00073.

3. Groh, C., Tautz, J., and Rössler, W. (2004). Synaptic organization in the adult honey bee brain is influenced by brood-temperature control during pupal development. Proc. Natl. Acad. Sci. *101*, 4268–4273. https://doi.org/10.1073/pnas.0400773101.

4. Wang, G., Gordon, T.N., and Rainwater, S. (2008). Maximum voluntary temperature of insect larvae reveals differences in their thermal biology. J. Therm. Biol. *33*, 380–384. https://doi.org/10.1016/j.jtherbio.2008.06.002.

5. Züfle, P., Batista, L.L., Brandão, S.C., D'Uva, G., Christian, D., and Martelli, C. (2023). Metabolic constraints on growth explain how developmental temperature scales synaptic connectivity relevant for behaviour. Preprint, https://doi.org/10.1101/2023.10.15.562389 https://doi.org/10.1101/2023.10.15.562389.

6. Baleba, S.B.S., Mahadevan, V.P., Knaden, M., and Hansson, B.S. (2023). Temperature-dependent modulation of odor-dependent behavior in three drosophilid fly species of differing thermal preference. Commun. Biol. *6*, 905. https://doi.org/10.1038/s42003-023-05280-5.

7. Becher, M.A., Scharpenberg, H., and Moritz, R.F.A. (2009). Pupal developmental temperature and behavioral specialization of honeybee workers (Apis mellifera L.). J. Comp. Physiol. A *195*, 673–679. https://doi.org/10.1007/s00359-009-0442-7.

8. Tautz, J., Maier, S., Groh, C., Rössler, W., and Brockmann, A. (2003). Behavioral performance in adult honey bees is influenced by the temperature experienced during their pupal development. Proc. Natl. Acad. Sci. *100*, 7343–7347. https://doi.org/10.1073/pnas.1232346100.

9. Weidenmüller, A., Mayr, C., Kleineidam, C.J., and Roces, F. (2009). Preimaginal and Adult Experience Modulates the Thermal Response Behavior of Ants. Curr. Biol. *19*, 1897–1902. https://doi.org/10.1016/j.cub.2009.08.059.

10. Jones, J.C., and Oldroyd, B.P. (2006). Nest Thermoregulation in Social Insects. In Advances in Insect Physiology (Elsevier), pp. 153–191. https://doi.org/10.1016/S0065-2806(06)33003-2.

11. Noble, D.W.A., Stenhouse, V., Riley, J.L., Warner, D.A., While, G.M., Du, W.-G., Uller, T., and Schwanz, L.E. (2018). A comprehensive database of thermal developmental plasticity in reptiles. Sci. Data *5*, 180138. https://doi.org/10.1038/sdata.2018.138.

12. Ohmer, M.E.B., Hammond, T.T., Switzer, S., Wantman, T., Bednark, J.G., Paciotta, E., Coscia, J., and Richards-Zawacki, C.L. (2023). Developmental environment has lasting effects on amphibian post-metamorphic behavior and thermal physiology. J. Exp. Biol. *226*, jeb244883. https://doi.org/10.1242/jeb.244883.

13. Crisp, S., Evers, J.F., Fiala, A., and Bate, M. (2008). The development of motor coordination in *Drosophila* embryos. Development *135*, 3707–3717. https://doi.org/10.1242/dev.026773.

14. Crisp, S.J., Evers, J.F., and Bate, M. (2011). Endogenous Patterns of Activity Are Required for the Maturation of a Motor Network. J. Neurosci. *31*, 10445–10450. https://doi.org/10.1523/JNEUROSCI.0346-11.2011.

15. Giachello, C.N.G., and Baines, R.A. (2015). Inappropriate Neural Activity during a Sensitive Period in Embryogenesis Results in Persistent Seizure-like Behavior. Curr. Biol. *25*, 2964–2968. https://doi.org/10.1016/j.cub.2015.09.040.

16. Williamson, M., Mitchell, A., and Condron, B. (2021). Birth temperature followed by a visual critical period determines cooperative group membership. J. Comp. Physiol. A *207*, 739–746. https://doi.org/10.1007/s00359-021-01512-3.

17. Krick, N., Davies, J., Coulson, B., Sobrido-Cameán, D., Miller, M., Oswald, M.C.W., Zarin, A.A., Baines, R., and Landgraf, M. (2024). Heterogeneous responses to embryonic critical period

perturbations among different components of the *Drosophila* larval locomotor circuit. Preprint, https://doi.org/10.1101/2024.09.14.613036 https://doi.org/10.1101/2024.09.14.613036.

18. Hunter, I., Coulson, B., Pettini, T., Davies, J.J., Parkin, J., Landgraf, M., and Baines, R.A. (2024). Balance of activity during a critical period tunes a developing network. eLife *12*, RP91599. https://doi.org/10.7554/eLife.91599.

19. Marley, R., and Baines, R.A. (2011). Increased persistent Na^+ current contributes to seizure in the slamdance bang-sensitive *Drosophila* mutant. J. Neurophysiol. *106*, 18–29. https://doi.org/10.1152/jn.00808.2010.

20. Carreira-Rosario, A., York, R.A., Choi, M., Doe, C.Q., and Clandinin, T.R. (2021). Mechanosensory input during circuit formation shapes Drosophila motor behavior through patterned spontaneous network activity. Curr. Biol. *31*, 5341-5349.e4. https://doi.org/10.1016/j.cub.2021.08.022.

21. Zeng, X., Komanome, Y., Kawasaki, T., Inada, K., Jonaitis, J., Pulver, S.R., Kazama, H., and Nose, A. (2021). An electrically coupled pioneer circuit enables motor development via proprioceptive feedback in Drosophila embryos. Curr. Biol. *31*, 5327-5340.e5. https://doi.org/10.1016/j.cub.2021.10.005.

22. Truszkowski, T.L.S., and Aizenman, C.D. (2015). Neurobiology: Setting the Set Point for Neural Homeostasis. Curr. Biol. *25*, R1132–R1133. https://doi.org/10.1016/j.cub.2015.10.021.

23. Giachello, C.N.G., Fan, Y.N., Landgraf, M., and Baines, R.A. (2021). Nitric oxide mediates activity-dependent change to synaptic excitation during a critical period in Drosophila. Sci. Rep. *11*, 20286. https://doi.org/10.1038/s41598-021-99868-8.

24. Somero, G.N., Lockwood, B.L., and Tomanek, L. (2017). Biochemical adaptation: response to environmental challenges from life's origins to the Anthropocene (Sinauer associates, Inc. publishers).

25. Scialò, F., Sriram, A., Fernández-Ayala, D., Gubina, N., Lõhmus, M., Nelson, G., Logan, A., Cooper, H.M., Navas, P., Enríquez, J.A., et al. (2016). Mitochondrial ROS Produced via Reverse Electron Transport Extend Animal Lifespan. Cell Metab. *23*, 725–734. https://doi.org/10.1016/j.cmet.2016.03.009.

26. Scialò, F., Fernández-Ayala, D.J., and Sanz, A. (2017). Role of Mitochondrial Reverse Electron Transport in ROS Signaling: Potential Roles in Health and Disease. Front. Physiol. *8*, 428. https://doi.org/10.3389/fphys.2017.00428.

27. Scialò, F., Sriram, A., Stefanatos, R., Spriggs, R.V., Loh, S.H.Y., Martins, L.M., and Sanz, A. (2020). Mitochondrial complex I derived ROS regulate stress adaptation in Drosophila melanogaster. Redox Biol. *32*, 101450. https://doi.org/10.1016/j.redox.2020.101450.

28. Sanz, A., Soikkeli, M., Portero-Otín, M., Wilson, A., Kemppainen, E., McIlroy, G., Ellilä, S., Kemppainen, K.K., Tuomela, T., Lakanmaa, M., et al. (2010). Expression of the yeast NADH dehydrogenase Ndi1 in *Drosophila* confers increased lifespan independently of dietary restriction. Proc. Natl. Acad. Sci. *107*, 9105–9110. https://doi.org/10.1073/pnas.0911539107.

29. Sanz, A., Stefanatos, R., and McIlroy, G. (2010). Production of reactive oxygen species by the mitochondrial electron transport chain in Drosophila melanogaster. J. Bioenerg. Biomembr. *42*, 135–142. https://doi.org/10.1007/s10863-010-9281-z.

30. Chandel, N.S., McClintock, D.S., Feliciano, C.E., Wood, T.M., Melendez, J.A., Rodriguez, A.M., and Schumacker, P.T. (2000). Reactive Oxygen Species Generated at Mitochondrial Complex III Stabilize Hypoxia-inducible Factor-1α during Hypoxia. J. Biol. Chem. *275*, 25130–25138. https://doi.org/10.1074/jbc.M001914200.

31. Movafagh, S., Crook, S., and Vo, K. (2015). Regulation of Hypoxia-Inducible Factor-1a by Reactive Oxygen Species : New Developments in an Old Debate: Regulation of Hypoxia-Inducible Factor-1a. J. Cell. Biochem. *116*, 696–703. https://doi.org/10.1002/jcb.25074.

32. Qutub, A.A., and Popel, A.S. (2008). Reactive Oxygen Species Regulate Hypoxia-Inducible Factor 1α Differentially in Cancer and Ischemia. Mol. Cell. Biol. *28*, 5106–5119. https://doi.org/10.1128/MCB.00060-08.

33. Huang, X., Zhao, L., and Peng, R. (2022). Hypoxia-Inducible Factor 1 and Mitochondria: An Intimate Connection. Biomolecules *13*, 50. https://doi.org/10.3390/biom13010050.

34. Tomita, S., Ueno, M., Sakamoto, M., Kitahama, Y., Ueki, M., Maekawa, N., Sakamoto, H., Gassmann, M., Kageyama, R., Ueda, N., et al. (2003). Defective Brain Development in Mice Lacking the *Hif-1* α Gene in Neural Cells. Mol. Cell. Biol. *23*, 6739–6749. https://doi.org/10.1128/MCB.23.19.6739-6749.2003.

35. Semenza, G.L. (2006). Regulation of physiological responses to continuous and intermittent hypoxia by hypoxia-inducible factor 1. Exp. Physiol. *91*, 803–806. https://doi.org/10.1113/expphysiol.2006.033498.

36. Milosevic, J., Maisel, M., Wegner, F., Leuchtenberger, J., Wenger, R.H., Gerlach, M., Storch, A., and Schwarz, J. (2007). Lack of Hypoxia-Inducible Factor-1α Impairs Midbrain Neural Precursor Cells Involving Vascular Endothelial Growth Factor Signaling. J. Neurosci. *27*, 412–421. https://doi.org/10.1523/JNEUROSCI.2482-06.2007.

37. Iacobini, C., Vitale, M., Pugliese, G., and Menini, S. (2023). The “sweet” path to cancer: focus on cellular glucose metabolism. Front. Oncol. *13*, 1202093. https://doi.org/10.3389/fonc.2023.1202093.

38. Collins, C.A., Wairkar, Y.P., Johnson, S.L., and DiAntonio, A. (2006). Highwire Restrains Synaptic Growth by Attenuating a MAP Kinase Signal. Neuron *51*, 57–69. https://doi.org/10.1016/j.neuron.2006.05.026.

39. Shen, W., and Ganetzky, B. (2009). Autophagy promotes synapse development in *Drosophila*. J. Cell Biol. *187*, 71–79. https://doi.org/10.1083/jcb.200907109.

40. Frank, C.A., Wang, X., Collins, C.A., Rodal, A.A., Yuan, Q., Verstreken, P., and Dickman, D.K. (2013). New Approaches for Studying Synaptic Development, Function, and Plasticity Using *Drosophila* as a Model System. J. Neurosci. *33*, 17560–17568. https://doi.org/10.1523/JNEUROSCI.3261-13.2013.

41. Oswald, M.C., Brooks, P.S., Zwart, M.F., Mukherjee, A., West, R.J., Giachello, C.N., Morarach, K., Baines, R.A., Sweeney, S.T., and Landgraf, M. (2018). Reactive oxygen species regulate activity-dependent neuronal plasticity in Drosophila. eLife *7*, e39393. https://doi.org/10.7554/eLife.39393.

42. Sobrido-Cameán, D., Oswald, M.C.W., Bailey, D.M.D., Mukherjee, A., and Landgraf, M. (2023). Activity-regulated growth of motoneurons at the neuromuscular junction is mediated by NADPH oxidases. Front. Cell. Neurosci. *16*, 1106593. https://doi.org/10.3389/fncel.2022.1106593.

43. McDonald, A.E., and Vanlerberghe, G.C. (2004). Branched Mitochondrial Electron Transport in the Animalia: Presence of Alternative Oxidase in Several Animal Phyla. IUBMB Life *56*, 333–341. https://doi.org/10.1080/1521-6540400000876.

44. McDonald, A.E., Vanlerberghe, G.C., and Staples, J.F. (2009). Alternative oxidase in animals: unique characteristics and taxonomic distribution. J. Exp. Biol. *212*, 2627–2634. https://doi.org/10.1242/jeb.032151.

45. Matus-Ortega, M.G., Salmerón-Santiago, K.G., Flores-Herrera, O., Guerra-Sánchez, G., Martínez, F., Rendón, J.L., and Pardo, J.P. (2011). The alternative NADH dehydrogenase is present in mitochondria of some animal taxa. Comp. Biochem. Physiol. Part D Genomics Proteomics *6*, 256–263. https://doi.org/10.1016/j.cbd.2011.05.002.

46. Weaver, R.J., and McDonald, A.E. (2023). Mitochondrial alternative oxidase across the tree of life: Presence, absence, and putative cases of lateral gene transfer. Biochim. Biophys. Acta BBA - Bioenerg. *1864*, 149003. https://doi.org/10.1016/j.bbabio.2023.149003.

47. Maxwell, D.P., Wang, Y., and McIntosh, L. (1999). The alternative oxidase lowers mitochondrial reactive oxygen production in plant cells. Proc. Natl. Acad. Sci. *96*, 8271–8276. https://doi.org/10.1073/pnas.96.14.8271.

48. Fernandez-Ayala, D.J.M., Sanz, A., Vartiainen, S., Kemppainen, K.K., Babusiak, M., Mustalahti, E., Costa, R., Tuomela, T., Zeviani, M., Chung, J., et al. (2009). Expression of the Ciona intestinalis Alternative Oxidase (AOX) in Drosophila Complements Defects in Mitochondrial Oxidative Phosphorylation. Cell Metab. *9*, 449–460. https://doi.org/10.1016/j.cmet.2009.03.004.

49. El-Khoury, R., Dufour, E., Rak, M., Ramanantsoa, N., Grandchamp, N., Csaba, Z., Duvillié, B., Bénit, P., Gallego, J., Gressens, P., et al. (2013). Alternative Oxidase Expression in the Mouse Enables Bypassing Cytochrome c Oxidase Blockade and Limits Mitochondrial ROS Overproduction. PLoS Genet. *9*, e1003182. https://doi.org/10.1371/journal.pgen.1003182.

50. Pfeiffer, B.D., Jenett, A., Hammonds, A.S., Ngo, T.-T.B., Misra, S., Murphy, C., Scully, A., Carlson, J.W., Wan, K.H., Laverty, T.R., et al. (2008). Tools for neuroanatomy and neurogenetics in *Drosophila*. Proc. Natl. Acad. Sci. *105*, 9715–9720. https://doi.org/10.1073/pnas.0803697105.

51. Liu, K., Jones, S., Minis, A., Rodriguez, J., Molina, H., and Steller, H. (2019). PI31 Is an Adaptor Protein for Proteasome Transport in Axons and Required for Synaptic Development. Dev. Cell *50*, 509-524.e10. https://doi.org/10.1016/j.devcel.2019.06.009.

52. McClure, C.D., Hassan, A., Aughey, G.N., Butt, K., Estacio-Gómez, A., Duggal, A., Ying Sia, C., Barber, A.F., and Southall, T.D. (2022). An auxin-inducible, GAL4-compatible, gene expression system for Drosophila. eLife *11*, e67598. https://doi.org/10.7554/eLife.67598.

53. Weidemann, A., and Johnson, R.S. (2008). Biology of HIF-1α. Cell Death Differ. *15*, 621–627. https://doi.org/10.1038/cdd.2008.12.

54. Strowitzki, M., Cummins, E., and Taylor, C. (2019). Protein Hydroxylation by Hypoxia-Inducible Factor (HIF) Hydroxylases: Unique or Ubiquitous? Cells *8*, 384. https://doi.org/10.3390/cells8050384.

55. Chandel, N.S., Maltepe, E., Goldwasser, E., Mathieu, C.E., Simon, M.C., and Schumacker, P.T. (1998). Mitochondrial reactive oxygen species trigger hypoxia-induced transcription. Proc. Natl. Acad. Sci. *95*, 11715–11720. https://doi.org/10.1073/pnas.95.20.11715.

56. Brunelle, J.K., Bell, E.L., Quesada, N.M., Vercauteren, K., Tiranti, V., Zeviani, M., Scarpulla, R.C., and Chandel, N.S. (2005). Oxygen sensing requires mitochondrial ROS but not oxidative phosphorylation. Cell Metab. *1*, 409–414. https://doi.org/10.1016/j.cmet.2005.05.002.

57. Guzy, R.D., Hoyos, B., Robin, E., Chen, H., Liu, L., Mansfield, K.D., Simon, M.C., Hammerling, U., and Schumacker, P.T. (2005). Mitochondrial complex III is required for hypoxia-induced ROS production and cellular oxygen sensing. Cell Metab. *1*, 401–408. https://doi.org/10.1016/j.cmet.2005.05.001.

58. Fuhrmann, D.C., and Brüne, B. (2017). Mitochondrial composition and function under the control of hypoxia. Redox Biol. *12*, 208–215. https://doi.org/10.1016/j.redox.2017.02.012.

59. Walton, K.D., Lieberman, D., Llinás, A., Begin, M., and Llinás, R.R. (1992). Identification of a critical period for motor development in neonatal rats. Neuroscience *51*, 763–767. https://doi.org/10.1016/0306-4522(92)90517-6.

60. Moorman, S.J., Cordova, R., and Davies, S.A. (2002). A critical period for functional vestibular development in zebrafish. Dev. Dyn. *223*, 285–291. https://doi.org/10.1002/dvdy.10052.

61. Avitan, L., Pujic, Z., Mölter, J., Van De Poll, M., Sun, B., Teng, H., Amor, R., Scott, E.K., and Goodhill, G.J. (2017). Spontaneous Activity in the Zebrafish Tectum Reorganizes over Development and Is Influenced by Visual Experience. Curr. Biol. *27*, 2407-2419.e4. https://doi.org/10.1016/j.cub.2017.06.056.

62. Xie, J., Jusuf, P.R., Bui, B.V., and Goodbourn, P.T. (2019). Experience-dependent development of visual sensitivity in larval zebrafish. Sci. Rep. *9*, 18931. https://doi.org/10.1038/s41598-019-54958-6.

63. Chin, J.S.R., Phan, T.-A.N., Albert, L.T., Keene, A.C., and Duboué, E.R. (2022). Long lasting anxiety following early life stress is dependent on glucocorticoid signaling in zebrafish. Sci. Rep. *12*, 12826. https://doi.org/10.1038/s41598-022-16257-5.

64. Hageter, J., Starkey, J., and Horstick, E.J. (2023). Thalamic regulation of a visual critical period and motor behavior. Cell Rep. *42*, 112287. https://doi.org/10.1016/j.celrep.2023.112287.

65. Coulson, B., Hunter, I., Doran, S., Parkin, J., Landgraf, M., and Baines, R.A. (2022). Critical periods in Drosophila neural network development: Importance to network tuning and therapeutic potential. Front. Physiol. *13*, 1073307. https://doi.org/10.3389/fphys.2022.1073307.

66. Reh, R.K., Dias, B.G., Nelson, C.A., Kaufer, D., Werker, J.F., Kolb, B., Levine, J.D., and Hensch, T.K. (2020). Critical period regulation across multiple timescales. Proc. Natl. Acad. Sci. *117*, 23242–23251. https://doi.org/10.1073/pnas.1820836117.

67. Graham, C., Stefanatos, R., Yek, A.E.H., Spriggs, R.V., Loh, S.H.Y., Uribe, A.H., Zhang, T., Martins, L.M., Maddocks, O.D.K., Scialo, F., et al. (2022). Mitochondrial ROS signalling requires uninterrupted electron flow and is lost during ageing in flies. GeroScience. https://doi.org/10.1007/s11357-022-00555-x.

68. Mòdol, L., Moissidis, M., Selten, M., Oozeer, F., and Marín, O. (2024). Somatostatin interneurons control the timing of developmental desynchronization in cortical networks. Neuron *112*, 2015-2030.e5. https://doi.org/10.1016/j.neuron.2024.03.014.

69. Hensch, T.K. (2004). CRITICAL PERIOD REGULATION. Annu. Rev. Neurosci. *27*, 549–579. https://doi.org/10.1146/annurev.neuro.27.070203.144327.

70. Hensch, T.K. (2005). Critical period plasticity in local cortical circuits. Nat. Rev. Neurosci. *6*, 877–888. https://doi.org/10.1038/nrn1787.

71. Dhawan, S., Myers, P., Bailey, D.M.D., Ostrovsky, A.D., Evers, J.F., and Landgraf, M. (2021). Reactive Oxygen Species Mediate Activity-Regulated Dendritic Plasticity Through NADPH Oxidase and Aquaporin Regulation. Front. Cell. Neurosci. *15*, 641802. https://doi.org/10.3389/fncel.2021.641802.

72. Robb, E.L., Hall, A.R., Prime, T.A., Eaton, S., Szibor, M., Viscomi, C., James, A.M., and Murphy, M.P. (2018). Control of mitochondrial superoxide production by reverse electron transport at complex I. J. Biol. Chem. *293*, 9869–9879. https://doi.org/10.1074/jbc.RA118.003647.

73. Styr, B., Gonen, N., Zarhin, D., Ruggiero, A., Atsmon, R., Gazit, N., Braun, G., Frere, S., Vertkin, I., Shapira, I., et al. (2019). Mitochondrial Regulation of the Hippocampal Firing Rate Set Point and Seizure Susceptibility. Neuron *102*, 1009-1024.e8. https://doi.org/10.1016/j.neuron.2019.03.045.

74. Vander Heiden, M.G., Cantley, L.C., and Thompson, C.B. (2009). Understanding the Warburg Effect: The Metabolic Requirements of Cell Proliferation. Science *324*, 1029–1033. https://doi.org/10.1126/science.1160809.

75. Wang, C.-W., Purkayastha, A., Jones, K.T., Thaker, S.K., and Banerjee, U. (2016). In vivo genetic dissection of tumor growth and the Warburg effect. eLife *5*, e18126. https://doi.org/10.7554/eLife.18126.

76. Elzakra, N., and Kim, Y. (2021). HIF-1α Metabolic Pathways in Human Cancer. In Cancer Metabolomics Advances in Experimental Medicine and Biology., S. Hu, ed. (Springer International Publishing), pp. 243–260. https://doi.org/10.1007/978-3-030-51652-9_17.

77. Dunwoodie, S.L. (2009). The Role of Hypoxia in Development of the Mammalian Embryo. Dev. Cell *17*, 755–773. https://doi.org/10.1016/j.devcel.2009.11.008.

78. Bohuslavova, R., Cerychova, R., Papousek, F., Olejnickova, V., Bartos, M., Görlach, A., Kolar, F., Sedmera, D., Semenza, G.L., and Pavlinkova, G. (2019). HIF-1α is required for development of the sympathetic nervous system. Proc. Natl. Acad. Sci. *116*, 13414–13423. https://doi.org/10.1073/pnas.1903510116.

79. Kallio, P.J. (1998). Signal transduction in hypoxic cells: inducible nuclear translocation and recruitment of the CBP/p300 coactivator by the hypoxia-inducible factor-1alpha. EMBO J. *17*, 6573–6586. https://doi.org/10.1093/emboj/17.22.6573.

80. Perez-Perri, J.I., Dengler, V.L., Audetat, K.A., Pandey, A., Bonner, E.A., Urh, M., Mendez, J., Daniels, D.L., Wappner, P., Galbraith, M.D., et al. (2016). The TIP60 Complex Is a Conserved Coactivator of HIF1A. Cell Rep. *16*, 37–47. https://doi.org/10.1016/j.celrep.2016.05.082.

81. Luo, W., and Wang, Y. (2018). Epigenetic regulators: multifunctional proteins modulating hypoxia-inducible factor-α protein stability and activity. Cell. Mol. Life Sci. *75*, 1043–1056. https://doi.org/10.1007/s00018-017-2684-9.

82. Yfantis, A., Mylonis, I., Chachami, G., Nikolaidis, M., Amoutzias, G.D., Paraskeva, E., and Simos, G. (2023). Transcriptional Response to Hypoxia: The Role of HIF-1-Associated Co-Regulators. Cells *12*, 798. https://doi.org/10.3390/cells12050798.

83. Sulkowski, M.J., Han, T.H., Ott, C., Wang, Q., Verheyen, E.M., Lippincott-Schwartz, J., and Serpe, M. (2016). A Novel, Noncanonical BMP Pathway Modulates Synapse Maturation at the

Drosophila Neuromuscular Junction. PLOS Genet. *12,* e1005810. https://doi.org/10.1371/journal.pgen.1005810.

84. Bataillé, L., Delon, I., Da Ponte, J. P., Brown, N. H., & Jagla, K. (2010). Downstream of identity genes: muscle-type-specific regulation of the fusion process. Developmental cell, 19(2), 317–328. https://doi.org/10.1016/j.devcel.2010.07.008

85. Fujioka, M., Lear, B. C., Landgraf, M., Yusibova, G. L., Zhou, J., Riley, K. M., et al. (2003). Even-skipped, acting as a repressor, regulates axonal projections in Drosophila. Development 130, 5385–5400. https://doi: 10.1242/dev.00770

Figures

Figure 1. Mitochondrial ROS generated by reverse electron transport in muscles are necessary for critical period heat stress to change NMJ development.

A) Experimental paradigm

B) Heat stress experienced during the embryonic critical period (32°C *vs* 25°C control) leads to increased aCC NMJ terminal size and decreased postsynaptic GluRIIA, while not affecting subunit GluRIIB expression. Simultaneous genetic manipulation of muscle DA1 during embryonic stages only identifies mitochondrial ROS generated by reverse electron transport as necessary signals. "Control" indicates control genotype heterozygous for Oregon-R and DA1-Gal4. Larvae were reared at the control temperature of 25°C until the late wandering stage, 100 hrs after larval hatching (ALH). GluRIIA and GluRIIB subunits are displayed with lookup table "fire" to illustrate signal intensities (warmer colours indicating greater signal intensities). Scale bar = 20 μm.

C) Dot-plot quantification shows changes to aCC NMJ growth on its target muscle DA1, based on the standard measure of the number of boutons (swellings containing multiple presynaptic release sites/active zones). Data are shown with mean ± SEM, ANOVA, *** $p<0.0001$, **** $p<0.00001$, 'ns' indicates statistical non-significance. Black asterisks indicate comparison with the control condition of 25°C throughout, genetically unmanipulated. Red asterisks indicate comparisons with control genotype exposed to 32°C heat stress during the embryonic critical period.

D) Dot-plot quantification shows changes in levels of the GluRIIA receptor subunit at aCC NMJs quantified in C). Data are shown with mean ± SEM, ANOVA, **** $p<0.00001$, 'ns' indicates statistical non-significance. Black asterisks indicate comparison with the control condition of 25°C throughout, genetically unmanipulated. Red asterisks indicate comparisons with control genotype exposed to 32°C heat stress during the embryonic critical period.

E) Dot-plot quantification as in D), but for the low conductance GluRIIB receptor subunit, which remains unaffected by these manipulations.

A

embryo
L1
L3
CP
0h
0h ALH
100h ALH
25°C
32°C
25°C
DA1-Gal4

B

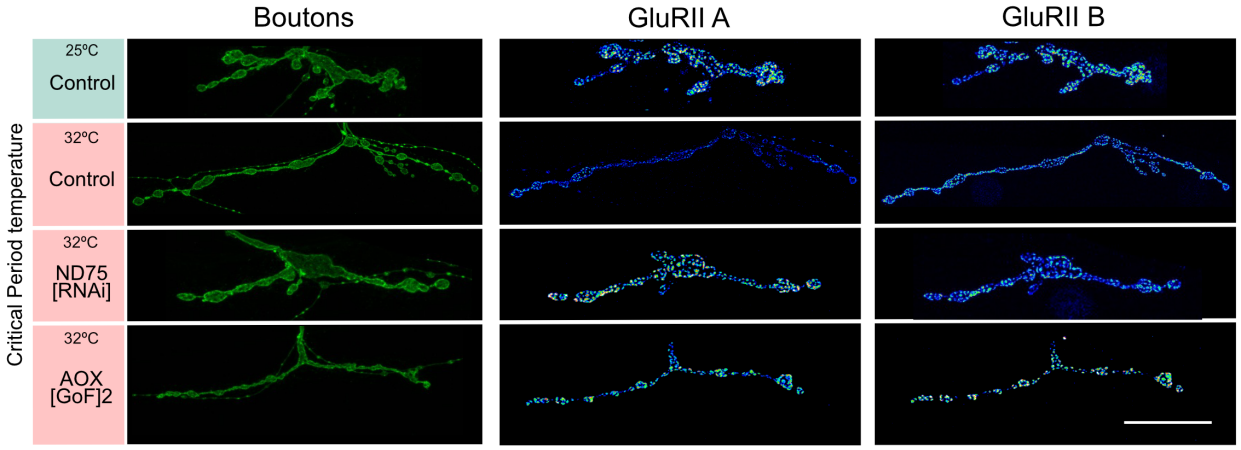
Boutons
GluRII A
GluRII B
Critical Period temperature
25ºC
Control
32ºC
Control
32ºC
ND75 [RNAi]
32ºC
AOX [GoF]2

C

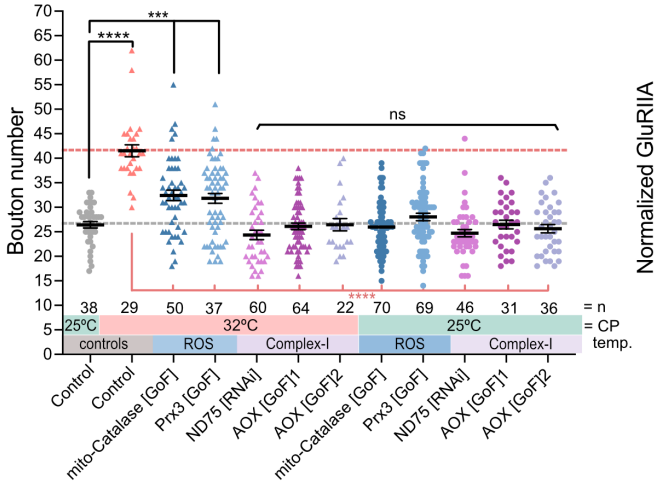
Bouton number
***
****
ns
****
38 29 50 37 60 64 22 70 69 46 31 36
= n
25ºC 32ºC 25ºC
= CP temp.
controls ROS Complex-I ROS Complex-I
Control
Control
mito-Catalase [GoF]
Prx3 [GoF]
ND75 [RNAi]
AOX [GoF]1
AOX [GoF]2
mito-Catalase [GoF]
Prx3 [GoF]
ND75 [RNAi]
AOX [GoF]1
AOX [GoF]2

D

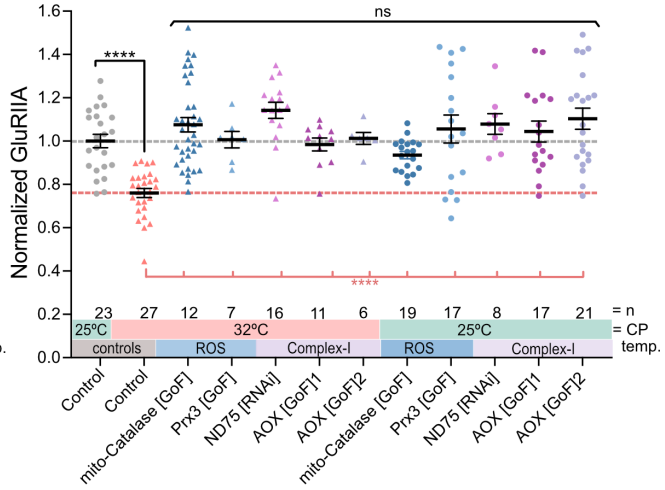
Normalized GluRIIA
ns
****
****
23 27 12 7 16 11 6 19 17 8 17 21
= n
25ºC 32ºC 25ºC
= CP temp.
controls ROS Complex-I ROS Complex-I
Control
Control
mito-Catalase [GoF]
Prx3 [GoF]
ND75 [RNAi]
AOX [GoF]1
AOX [GoF]2
mito-Catalase [GoF]
Prx3 [GoF]
ND75 [RNAi]
AOX [GoF]1
AOX [GoF]2

E

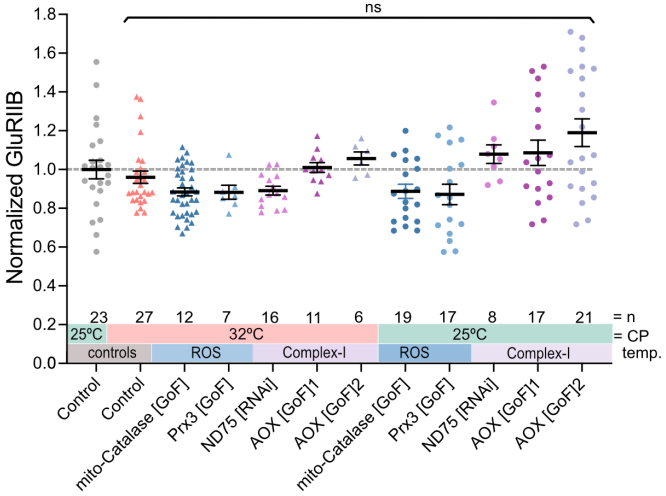
Normalized GluRIIB
ns
23 27 12 7 16 11 6 19 17 8 17 21
= n
25ºC 32ºC 25ºC
= CP temp.
controls ROS Complex-I ROS Complex-I
Control
Control
mito-Catalase [GoF]
Prx3 [GoF]
ND75 [RNAi]
AOX [GoF]1
AOX [GoF]2
mito-Catalase [GoF]
Prx3 [GoF]
ND75 [RNAi]
AOX [GoF]1
AOX [GoF]2

Figure 2: ROS by Complex-I, during the critical period, are sufficient to induce lasting changes to NMJ development.

A) Experimental paradigm

B) Induction of ROS at Complex-I via transient mis-expression of NDI1 in muscle DA1 during embryonic stages only phenocopies the effects that critical period heat stress has on subsequent NMJ development. "Control" indicates control genotype heterozygous for Oregon-R and DA1-Gal4. Larvae were reared at the control temperature of 25°C until the late wandering stage, 100 hrs ALH. GluRIIA and GluRIIB subunits are displayed with lookup table "fire" to illustrate signal intensities (warmer colours indicating greater signal intensities). Scale bar = 20 μm.

C) Dot-plot quantification shows changes to aCC NMJ growth on its target muscle DA1, based on the standard measure of the number of boutons (swellings containing multiple presynaptic release sites/active zones). Data are shown with mean ± SEM, ANOVA, *** $p<0.0001$, **** $p<0.00001$. Black asterisks indicate comparison with the control condition of 25°C throughout, genetically unmanipulated. Red asterisks indicate comparisons with control genotype exposed to 32°C heat stress during the embryonic critical period.

D) Dot-plot quantification shows changes in levels of the GluRIIA receptor subunit at aCC NMJs quantified in C). Data are shown with mean ± SEM, ANOVA, ** $p<0.001$, *** $p<0.0001$, 'ns' indicates statistical non-significance. Black asterisks indicate comparison with the control condition of 25°C throughout, genetically unmanipulated. Red asterisks indicate comparisons with control genotype exposed to 32°C heat stress during the embryonic critical period.

E) Dot-plot quantification as in D), but for the low conductance GluRIIB receptor subunit, which remains unaffected by these manipulations.

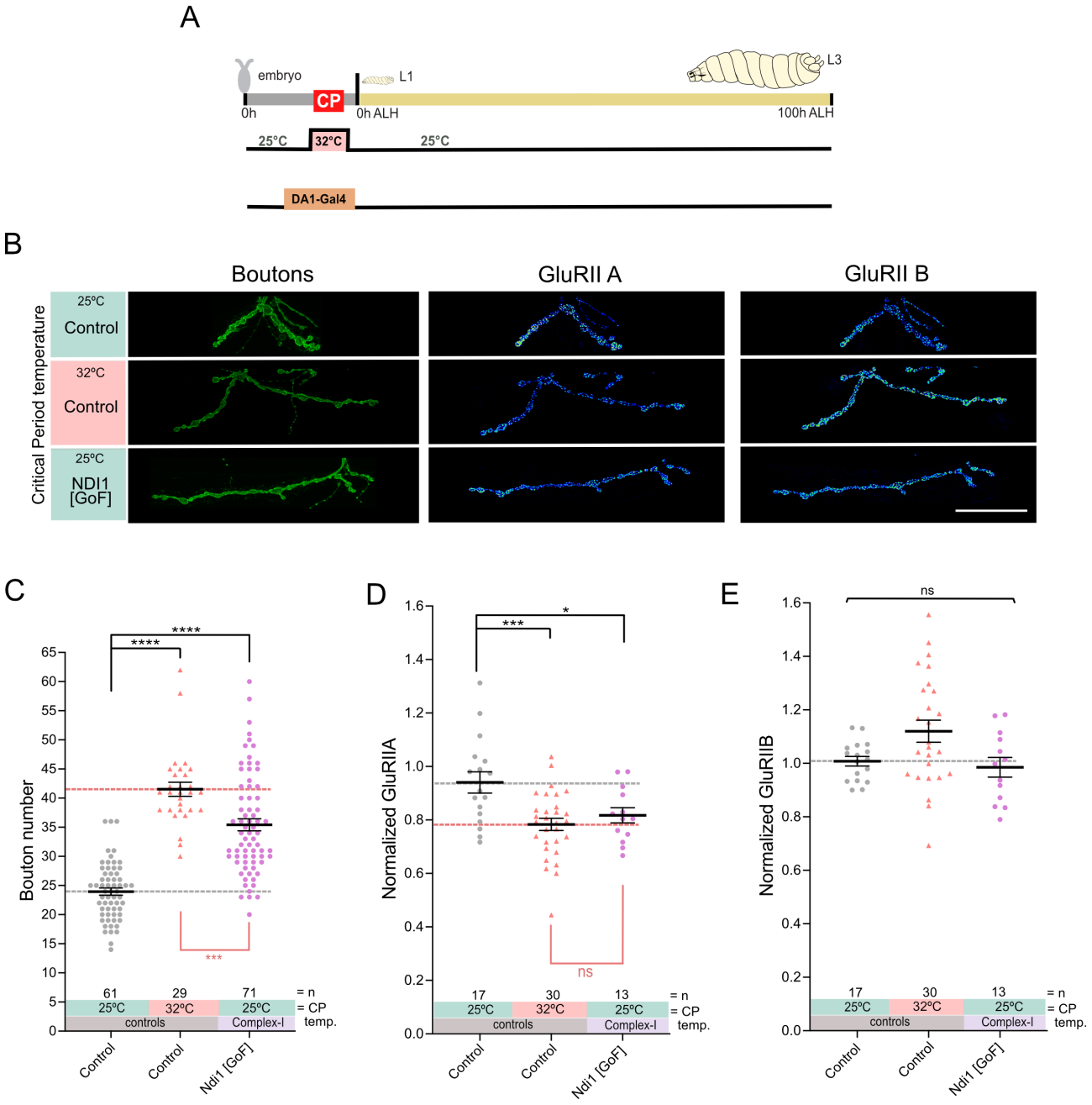
A
embryo
L1
L3
CP
0h
0h ALH
100h ALH
25°C
32°C
25°C
DA1-Gal4
B
Boutons
GluRII A
GluRII B
Critical Period temperature
25ºC
Control
32ºC
Control
25ºC
NDI1
[GoF]
C
Bouton number
****
****
***
61
29
71
= n
25ºC
32ºC
25ºC
= CP
controls
Complex-I
temp.
Control
Control
Ndi1 [GoF]
D
Normalized GluRIIA
***
*
ns
17
30
13
= n
25ºC
32ºC
25ºC
= CP
controls
Complex-I
temp.
Control
Control
Ndi1 [GoF]
E
Normalized GluRIIB
ns
17
30
13
= n
25ºC
32ºC
25ºC
= CP
controls
Complex-I
temp.
Control
Control
Ndi1 [GoF]

Figure 3: ROS by RET in embryonic motoneurons instructs subsequent NMJ development

A) Experimental paradigm

B) Temperature experienced during the embryonic critical period (25°C control *vs* 32°C heat stress) and simultaneous, transient genetic manipulation of motoneuron aCC during embryonic stages only via aCC-Gal4 [1] (aka*RN2-O-Gal4*). "Control" indicates control genotype heterozygous for Oregon-R and aCC-Gal4[1]. Larvae were reared at the control temperature of 25°C until the late wandering stage, 100 hrs ALH. Scale bar = 20 μm.

C) Dot-plot quantification shows changes to aCC NMJ growth on its target muscle DA1, based on the standard measure of the number of boutons (swellings containing multiple presynaptic release sites/active zones). Data are shown with mean ± SEM, ANOVA, **** $p<0.00001$, 'ns' indicates statistical non-significance. Black asterisks indicate comparison with the control condition of 25°C throughout, genetically unmanipulated. Red asterisks indicate comparisons with control genotype exposed to 32°C heat stress during the embryonic critical period.

D) Dot-plot quantification shows changes in number of the active zones at aCC NMJs quantified in C). Data are shown with mean ± SEM, ANOVA, **** $p<0.00001$, 'ns' indicates statistical non-significance. Black asterisks indicate comparison with the control condition of 25°C throughout, genetically unmanipulated. Red asterisks indicate comparisons with control genotype exposed to 32°C heat stress during the embryonic critical period.

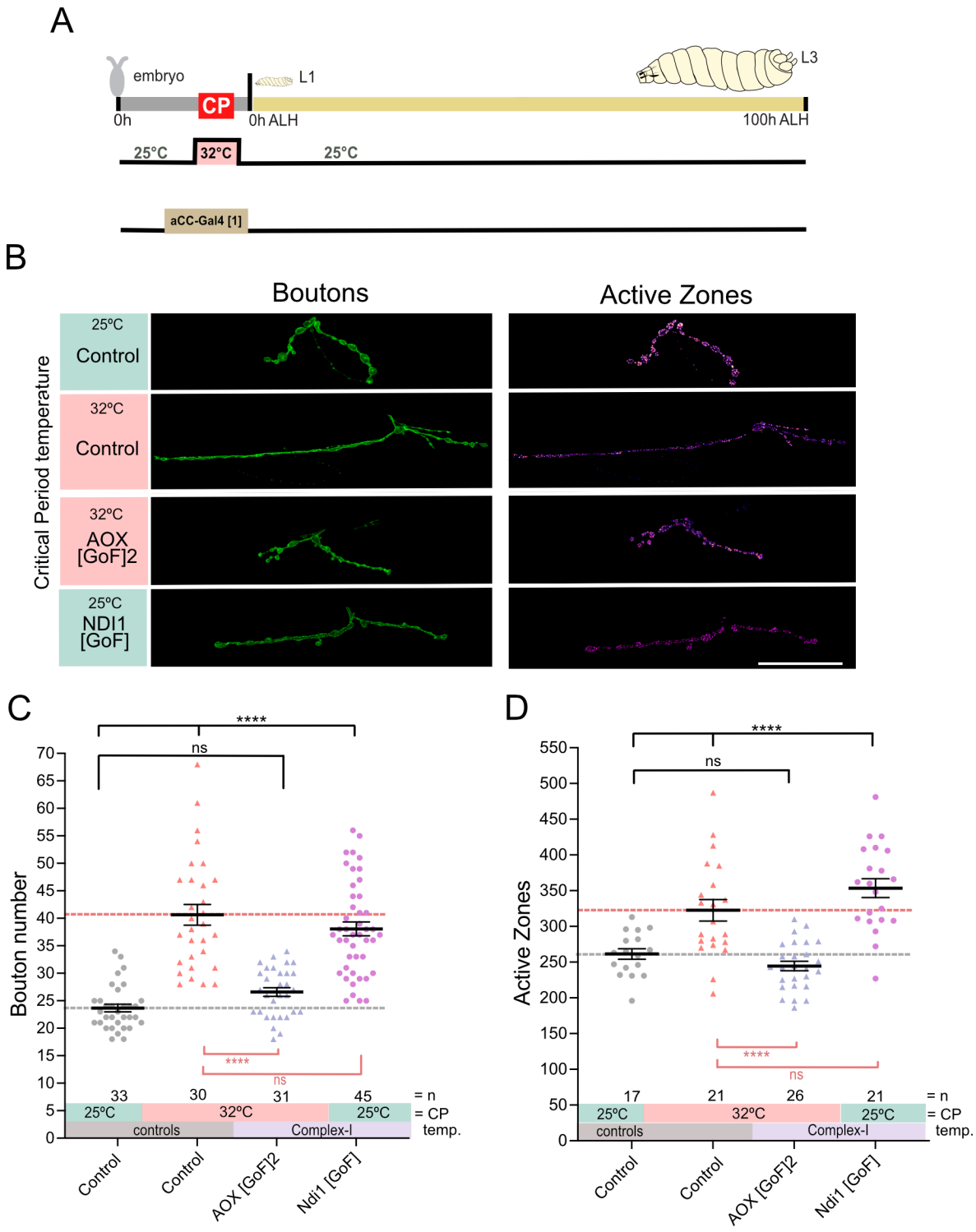
A
embryo
L1
L3
CP
0h
0h ALH
100h ALH
25°C
32°C
25°C
aCC-Gal4 [1]
B
Boutons
Active Zones
Critical Period temperature
25°C
Control
32°C
Control
32°C
AOX
[GoF]2
25°C
NDI1
[GoF]
C
Bouton number
****
ns
****
ns
33
30
31
45
= n
25°C
32°C
25°C
= CP
controls
Complex-I
temp.
Control
Control
AOX [GoF]2
Ndi1 [GoF]
D
Active Zones
****
ns
****
ns
17
21
26
21
= n
25°C
32°C
25°C
= CP
controls
Complex-I
temp.
Control
Control
AOX [GoF]2
Ndi1 [GoF]

Figure 4: HIF-1α is the signal downstream of ROS-RET.

A) Experimental paradigm

B) Temperature experienced during the embryonic critical period (25°C control *vs* 32°C heat stress) and simultaneous genetic manipulation of muscle DA1 during embryonic stages only. "Control" indicates control genotype heterozygous for Oregon-R and DA1-Gal4. Larvae were reared at the control temperature of 25°C until the late wandering stage, 100 hrs ALH. GluRIIA and GluRIIB subunits are displayed with lookup table "fire" to illustrate signal intensities (warmer colours indicating greater signal intensities). Scale bar = 20 μm.

C) Dot-plot quantification shows changes to aCC NMJ growth on its target muscle DA1, based on the standard measure of the number of boutons (swellings containing multiple presynaptic release sites/active zones). Data are shown with mean ± SEM, ANOVA, **** $p<0.00001$, 'ns' indicates statistical non-significance. Black asterisks indicate comparison with the control condition of 25°C throughout, genetically unmanipulated. Red asterisks indicate comparisons with control genotype exposed to 32°C heat stress during the embryonic critical period.

D) Dot-plot quantification shows changes in levels of the GluRIIA receptor subunit at aCC NMJs quantified in **C)**. Data are shown with mean ± SEM, ANOVA, * $p<0.01$, **** $p<0.00001$, 'ns' indicates statistical non-significance. Black asterisks indicate comparison with the control condition of 25°C throughout, genetically unmanipulated. Red asterisks indicate comparisons with control genotype exposed to 32°C heat stress during the embryonic critical period.

E) Dot-plot quantification as in **D)**, but for the low conductance GluRIIB receptor subunit, which remains unaffected by these manipulations.

A

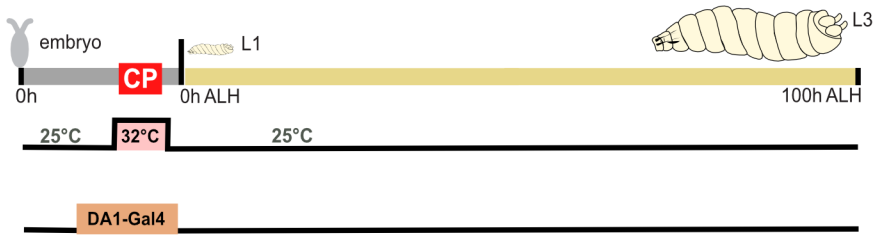
embryo
L1
L3
CP
0h
0h ALH
100h ALH
25°C
32°C
25°C
DA1-Gal4

B

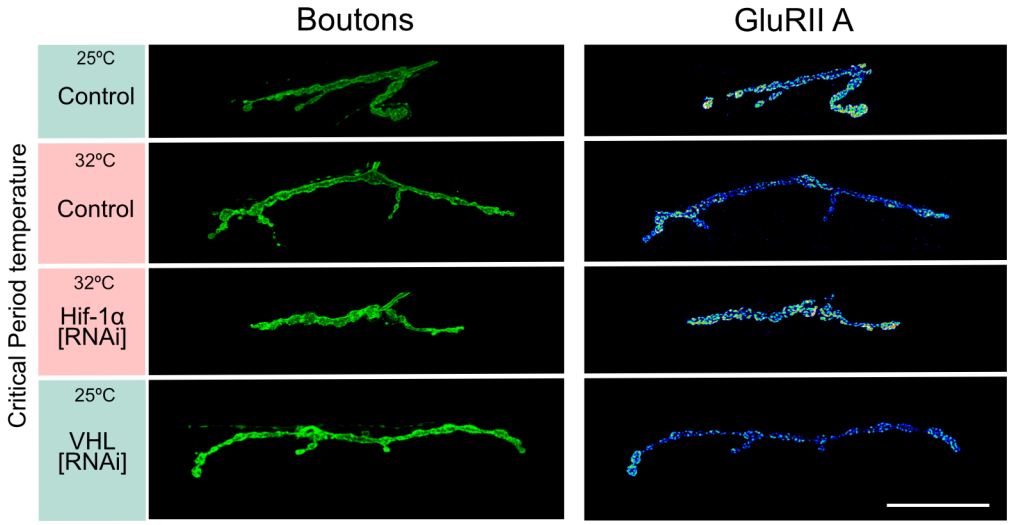
Boutons
GluRII A
Critical Period temperature
25ºC
Control
32ºC
Control
32ºC
Hif-1α
[RNAi]
25ºC
VHL
[RNAi]

C

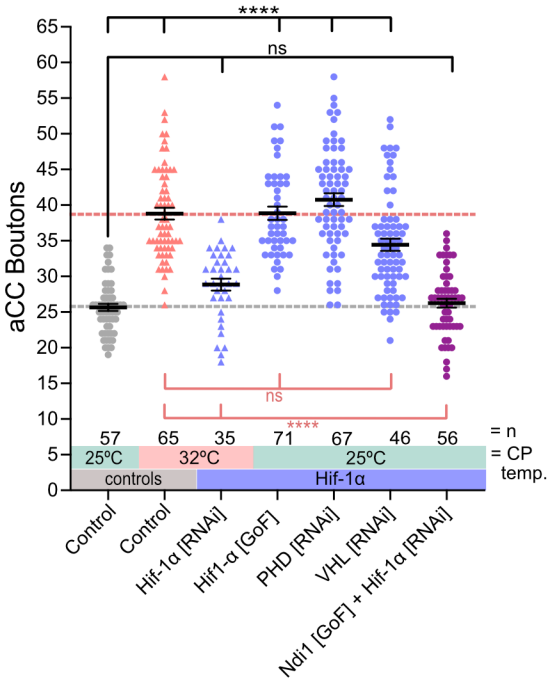
aCC Boutons
****
ns
ns
****
57 65 35 71 67 46 56
= n
25ºC 32ºC 25ºC
= CP temp.
controls
Hif-1α
Control
Control
Hif-1α [RNAi]
Hif1-α [GoF]
PHD [RNAi]
VHL [RNAi]
Ndi1 [GoF] + Hif-1α [RNAi]

D

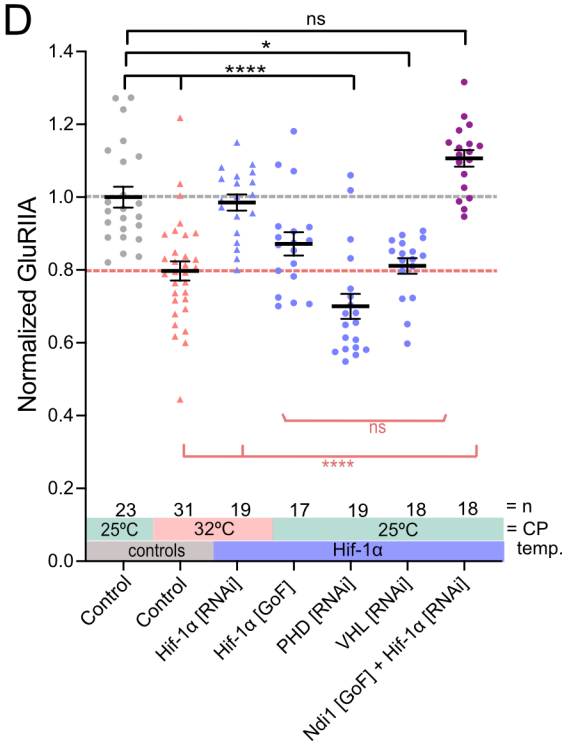
Normalized GluRIIA
ns
*
****
ns
****
23 31 19 17 19 18 18
= n
25ºC 32ºC 25ºC
= CP temp.
controls
Hif-1α
Control
Control
Hif-1α [RNAi]
Hif-1α [GoF]
PHD [RNAi]
VHL [RNAi]
Ndi1 [GoF] + Hif-1α [RNAi]

Figure 5. ROS by RET and HIF-1α signalling during the embryonic critical period are necessary and sufficient to reduce motoneuron excitability and crawling behaviour.

A) Experimental paradigm

B) aCC motoneuron excitability at the late third instar larval stage (i.e. action potential firing frequency triggered by current injected). Temperature experienced during the embryonic critical period (25°C control *vs* 32°C heat stress) and simultaneous transient genetic manipulation of aCC motoneuron during embryonic stages, via aCC-Gal4 [1] (RN2-O-Gal4). "Control" indicates control genotype heterozygous for Oregon-R and aCC-Gal4 [1]. Larvae were reared at the control temperature of 25°C until the late wandering stage, c. 100 hrs ALH. Control at 25°C *vs* 32°C is significant at $p = 0.0005$; Control at 25°C *vs* HIF-1α[GoF] is significant at $p = 0.0015$; Control at 25°C *vs* AOX[GoF]$_2$ at 32°C is not significant at $p = 0.28$.

C) Cell capacitance measurements as indicators of cell size show no significant differences between aCC motoneurons from specimens in B).

D) Resting membrane potential, as an indicator for cell integrity, show no significant differences between aCC motoneurons from specimens in B).

E) Crawling speed of third instar larvae (72 hrs ALH). Temperature experienced during the embryonic critical period (25°C control *vs* 32°C heat stress) and simultaneous genetic manipulation of CNS neurons during embryonic stages only. "Control" indicates control genotype heterozygous for Oregon-R and CNS-Gal4; Auxin-Gal80. Larvae were reared at the control temperature of 25°C. Each data point represents the crawling speed from an individual uninterrupted continuous forward crawl, n = specimen replicate number, up to three crawls assayed for each larva. Mean ± SEM, ANOVA, ns = not significant, ****$p<0.00001$.

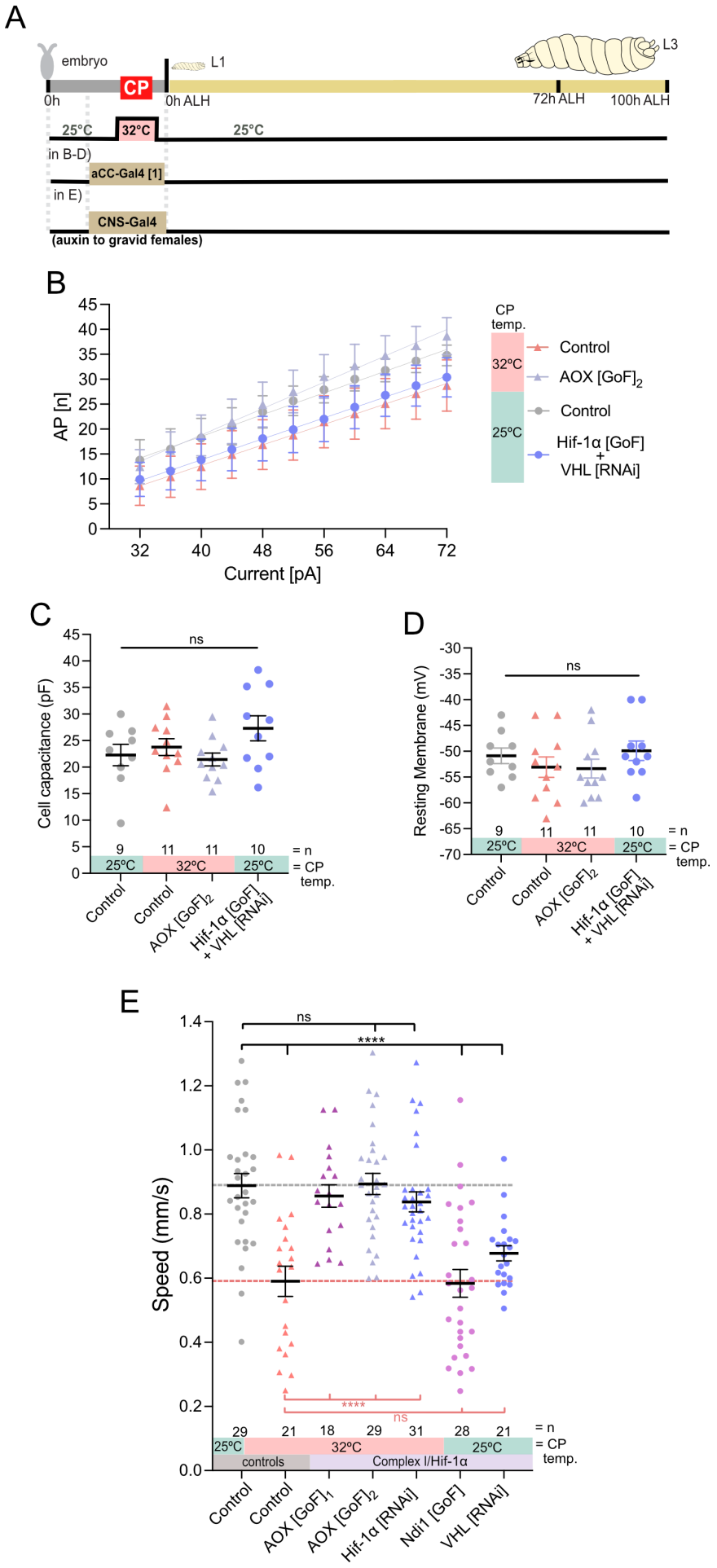
A
embryo
L1
L3
CP
0h
0h ALH
72h ALH
100h ALH
25°C
32°C
25°C
in B-D)
aCC-Gal4 [1]
in E)
CNS-Gal4
(auxin to gravid females)
B
AP [n]
Current [pA]
CP temp.
32°C
25°C
Control
AOX [GoF]2
Control
Hif-1α [GoF] + VHL [RNAi]
C
Cell capacitance (pF)
ns
9 11 11 10
= n
25°C 32°C 25°C
= CP temp.
Control
Control
AOX [GoF]2
Hif-1α [GoF] + VHL [RNAi]
D
Resting Membrane (mV)
ns
9 11 11 10
= n
25°C 32°C 25°C
= CP temp.
Control
Control
AOX [GoF]2
Hif-1α [GoF] + VHL [RNAi]
E
Speed (mm/s)
ns
****
****
ns
29 21 18 29 31 28 21
= n
25°C 32°C 25°C
= CP temp.
controls
Complex I/Hif-1α
Control
Control
AOX [GoF]1
AOX [GoF]2
Hif-1α [RNAi]
Ndi1 [GoF]
VHL [RNAi]

Figure 6. Working model

A) Heat stress during the critical period induces mitochondrial ROS, which lead to HIF-1α stabilisation and its accumulation in the nucleus, where HIF-1α generates long-lasting changes that impact on **B)** NMJ development: larger presynaptic terminals and less GluRIIA, as well as reductions in motoneuron excitability and, behaviourally, crawling speed.

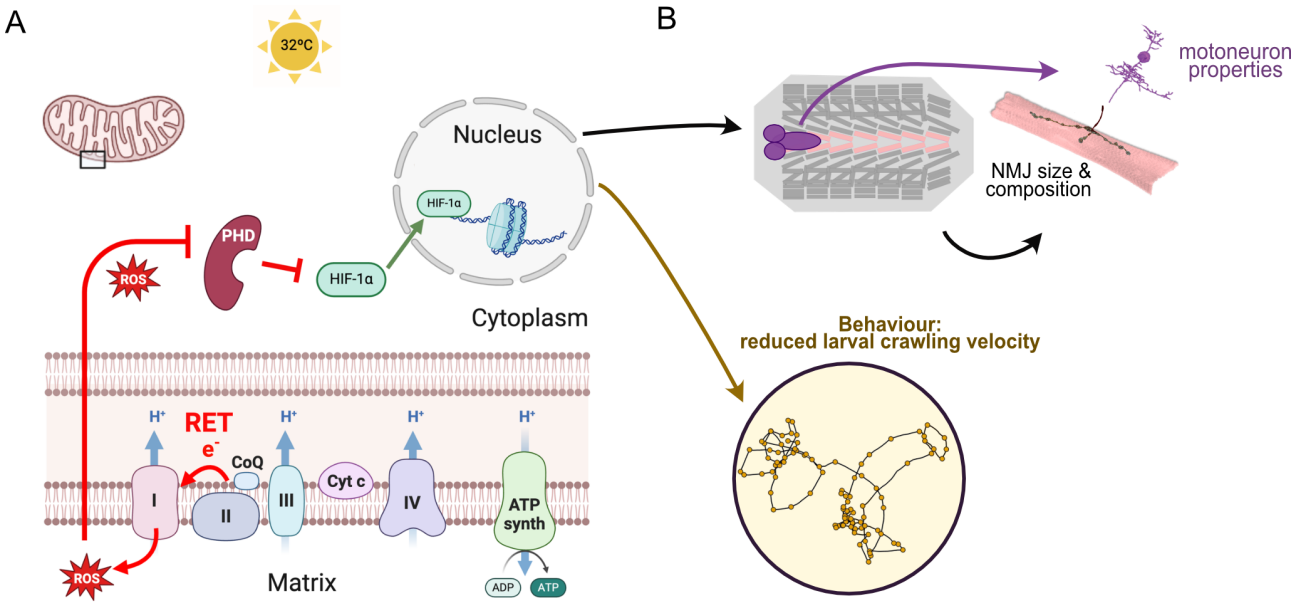

Tables

Table 1. Drosophila strains

Drosophila strain name	Additional information	Reference
Oregon-R-P2	Wild Type	Bloomington Drosophil Stock Center; RRID:BDSC_2376
eve-Gal4eme (aka SS2-C-Gal4)	Gal4 expression targeted to muscle DA1 during embryonic stages only	[84]
aka RN2-O-gal4 (aCC-Gal4 [1])	Gal4 expression targeted to motorneurons aCC and RP2 during embryonic stages only	[85]
GMR94G06-Gal4 (aCC-Gal4 [2])	Gal4 expression targeted to motorneuron aCC	Bloomington Drosophil Stock Center; RRID:BDSC_40701
GMR57C10-GAL4 (n-synaptobrevin-Gal4)	Gal4 expression targeted to neurons	Bloomington Drosophil Stock Center; RRID:BDSC_39171
AtTIR1-T2A-AID-GAL80-AID (Auxin-gal80)	Ubiquitously express GAL80 sensitive to auxin	[52]; gift from Tony Southall
UAS-mito-catalase	Mitochondrial targeted catalase under UAS control	gift from Alex Whitworth
UAS-Prx3	Peroxiredoxin 3 under UAS control	gift from Alberto Sanz
UAS-ND75 [RNAi]	Expresses dsRNA for RNAi of ND75 (FBgn0017566) under UAS control	Vienna Drosophila Resource Center #100733/KK; gift from Alberto Sanz
UAS-AOX [GoF]1	Expresses AOX from C. intestinalis under UAS control (allele F6)	[48]; gift from Alberto Sanz
UAS-AOX [GoF]2	Expresses AOX from C. intestinalis under UAS control (allele F24)	[48]; gift from Alberto Sanz
UAS-Ndi1 [GoF]	Expresses Ndi1 from S.cerevisae under UAS control (allele A46 and B20)	[28]; gift from Alberto Sanz
UAS-Sima [RNAi]	Expresses dsRNA for RNAi of sima (FBgn0266411) under UAS control	Bloomington Drosophil Stock Center; RRID:BDSC_26207
UAS-Sima [GoF]	Expresses sima (FBgn0266411) under UAS control	Gift from Joe Bateman
UAS-VHL [RNAi]	Expresses dsRNA for RNAi of VHL (FBgn0041174) under UAS control	Bloomington Drosophil Stock Center; RRID:BDSC_50727
UAS-PHD [RNAi]	Expresses dsRNA for RNAi of PHD (FBgn0264785) under UAS control	Bloomington Drosophil Stock Center; RRID:BDSC_34717

Author Contributions

Conceptualization: D.S.-C. and M.L; Investigation: D.S.-C., B.C., M.C.W.O. and T.P.; Writing – Original Draft: D.S.-C. and M.L; Writing – Review & Editing: D.S.-C., B.C, M.C.W.O., T.P., R.A.B. and M.L.; Supervision: R.A.B and M.L.; Funding Acquisition: D.S-C., R.A.B and M.L.

Author competing interests

The authors declare no competing interests.

Funding

D.S.-C. was supported by the European Molecular Biology Organization (EMBO) with a long-term EMBO fellowship (ALTF 62-2021). This work was supported by a Joint Wellcome Trust Investigator Award to R.A.B. and M.L. (217099/Z/19/Z).

Acknowledgments

The authors are grateful to Mihaela Serpe for the Rabbit polyclonal anti-GluRIIB antiserum. The authors are grateful to Tony Southall, Alex Whitworth, Joe Bateman and Alberto Sanz for generously providing fly stocks. Stocks obtained from the Bloomington Drosophila Stock Center (NIH P40OD018537) were used in this study. The nc82 monoclonal antibody was

obtained from the Developmental Studies Hybridoma Bank, created by the NICHD of the NIH and maintained at The University of Iowa, Department of Biology, Iowa City, IA 52242. The work benefited from the Imaging Facility, Department of Zoology, supported by Matt Wayland, and funds from a Wellcome Trust Equipment Grant (WT079204) with contributions by the Sir Isaac Newton Trust in Cambridge, including Research Grant [18.07ii(c)]. Work on this project benefited from the Manchester Fly Facility, established through funds from the University of Manchester and the Wellcome Trust (Grant 087742/Z/08/Z).

Supplementary Material

Supplementary figure 1. RET-ROS and HIF-1α signalling has lasting impact on NMJ only during the Critical Period.

A) Experimental paradigm

B) Genetic manipulation of motoneuron aCC during the critical period *vs* after critical period closure. "Control" indicates control genotype heterozygous for Oregon-R and aCC-Gal4[2]; Auxin-Gal80. Larvae were reared at the control temperature of 25°C until the late wandering stage, 100 hrs ALH. Scale bar = 20 μm.

C) Dot-plot quantification shows changes to aCC NMJ growth on its target muscle DA1, based on the standard measure of the number of boutons (swellings containing multiple presynaptic release sites/active zones). Data are shown with mean ± SEM, ANOVA, **** $p<0.00001$, 'ns' indicates statistical non-significance.

D) Dot-plot quantification shows changes in number of the active zones at aCC NMJs quantified in C). Data are shown with mean ± SEM, ANOVA, *** $p<0.0001$, **** $p<0.00001$, 'ns' indicates statistical non-significance.

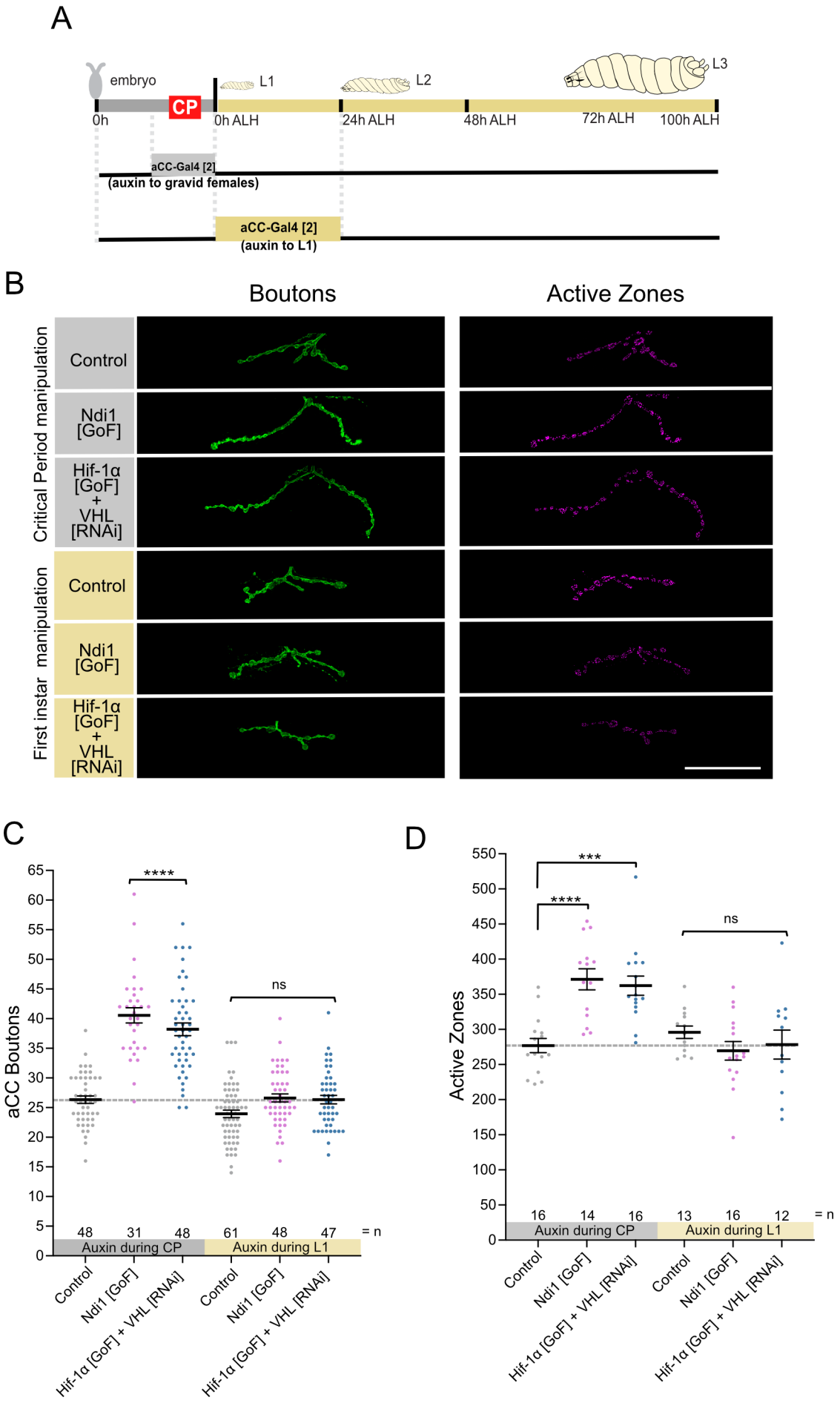
A
embryo
L1
L2
L3
CP
0h
0h ALH
24h ALH
48h ALH
72h ALH
100h ALH
aCC-Gal4 [2]
(auxin to gravid females)
aCC-Gal4 [2]
(auxin to L1)
B
Boutons
Active Zones
Critical Period manipulation
First instar manipulation
Control
Ndi1 [GoF]
Hif-1α [GoF] + VHL [RNAi]
Control
Ndi1 [GoF]
Hif-1α [GoF] + VHL [RNAi]
C
aCC Boutons
****
ns
48 31 48 61 48 47 = n
Auxin during CP
Auxin during L1
Control
Ndi1 [GoF]
Hif-1α [GoF] + VHL [RNAi]
Control
Ndi1 [GoF]
Hif-1α [GoF] + VHL [RNAi]
D
Active Zones
***
****
ns
16 14 16 13 16 12 = n
Auxin during CP
Auxin during L1
Control
Ndi1 [GoF]
Hif-1α [GoF] + VHL [RNAi]
Control
Ndi1 [GoF]
Hif-1α [GoF] + VHL [RNAi]

Supplementary figure 2. RET-ROS and HIF-1α signalling has not lasting impact on behaviour after the Critical Period.

A) Experimental paradigm
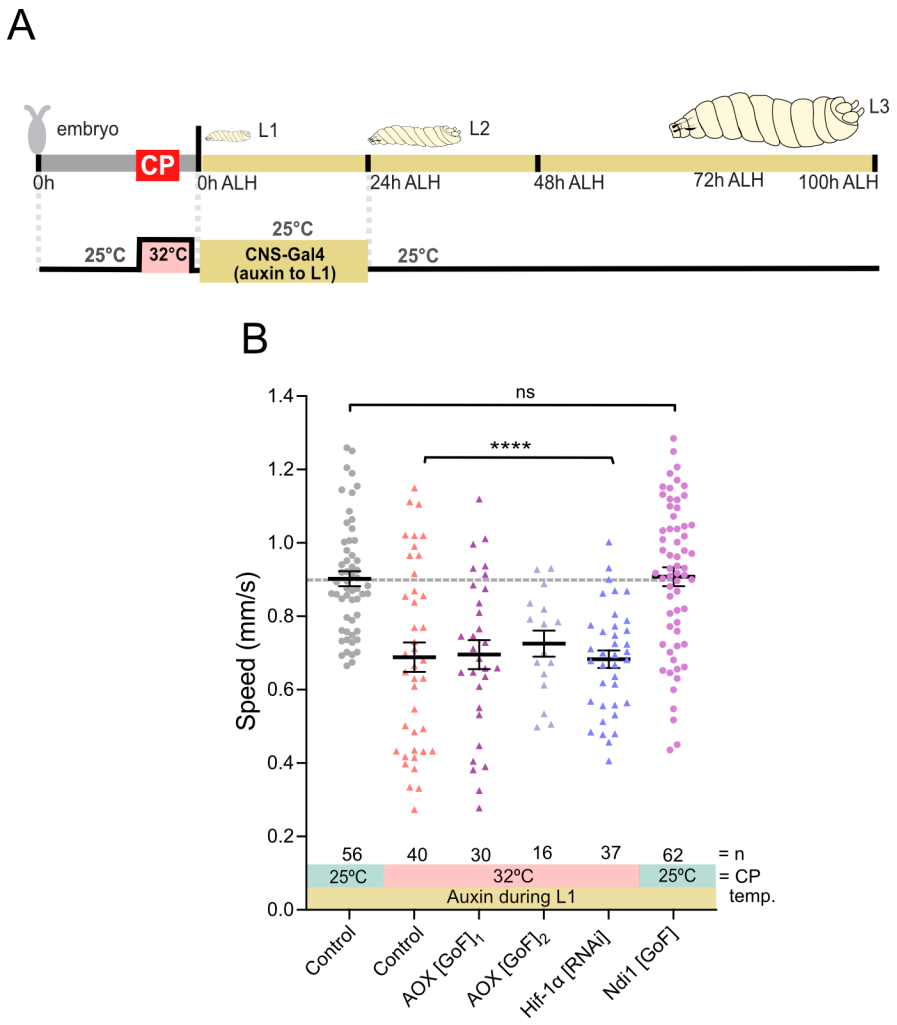
B) Crawling speed of third instar larvae (72 hrs after larval hatching (ALH)). Temperature experienced during the embryonic critical period (25°C control *vs* 32°C heat stress) and simultaneous genetic manipulation of all neurons during first instar stage. "Control" indicates control genotype heterozygous for Oregon-R and CNS-Gal4; Auxin-Gal80. Larvae were reared at the control temperature of 25°C until 72 hrs ALH. Each data point represents crawling speed from an individual uninterrupted continuous forward crawl, n = specimen replicate number, up to three crawls assayed for each larva. Mean ± SEM, ANOVA, ns = not significant, ****p<0.00001.